Joint Spatiotemporal Modes of Surface Temperature and Sea Level Pressure Variability in the Northern Hemisphere during the Last Century

MICHAEL E. MANN AND JEFFREY PARK

Department of Geology and Geophysics, Yale University, New Haven, Connecticut

ABSTRACT

Coherent spatiotemporal modes of climatic variability are isolated based on a multivariate frequency domain singular value decomposition (SVD) of nearly a century of monthly Northern Hemisphere sea level pressure (SLP) and surface temperature data. Insight into the underlying physical processes associated with potential climatic signals is obtained by examining the relationship between surface temperature and inferred atmospheric circulation patterns as they evolve over the a typical cycle, taking potential seasonal distinctions into account. Our analysis provides evidence for two significant independent secular variations describing a secular warming trend (and accompanying changes in circulation patterns) and a century timescale "oscillation" marked by high-amplitude variations in temperature and SLP in the North Atlantic that are similar to those observed in recent model simulations. Quasi-oscillatory interdecadal (16–18 yr timescale) variability also displays a pattern similar to those predicted in recent model experiments, with an apparent origin in the North Pacific. Weaker quasi-decadal (10–11-yr timescale), largely cold-season oscillatory behavior is more closely tied to the North Atlantic and may involve analogous mechanisms. Interannual variability is examined with an "evolutive" generalization of our procedure to captures the time-evolving frequency and amplitude characteristics of the associated climate signal. Variability exhibiting the characteristic climatic patterns of the global El Niño–Southern Oscillation (ENSO) phenomenon is described by two largely distinct frequency bands within the broader 3–7-yr ENSO band. The drifting central frequencies of these two dominant bands is suggestive of nonstationary behavior in ENSO. A quasibiennial signal exhibits a gradual trend toward increasing frequency. Prospects for improved long-range climate forecasting are discussed.

1. Introduction

In order to properly assess the potential impact of anthropogenic forcing of the climate, it is essential to identify the relative importance of the low-frequency natural variability that may arise from internal instabilities in the climate system. A number of recent studies have sought to identify such variability in instrumental climate records. While simultaneous analysis of multiple indices of climatic variability, including vertically resolved oceanographic and atmospheric data (see, e.g., Wallace et al. 1992; Fraedrich et al. 1993; Xu 1993), have the potential to offer the most insight, long duration (i.e., century-long) globally distributed records are not available. Several studies have analyzed century-long records of globally averaged (e.g., Folland et al. 1984; Kuo et al. 1990; Ghil and Vautard 1991; Schlesinger and Ramankutty 1994) or globally distributed (e.g., Mann and Park 1993, 1994, henceforth MP94; Allen and Smith 1994) temperature data in seeking to isolate potential climatic signals, including a potential greenhouse warming signal. For the Northern Hemisphere, widely distributed sea level pressure (SLP) data can supplement temperature data for almost a century, providing a potential means for investigating the dynamical influences governing large-scale climate variations.

While both univariate (e.g., Ghil and Vautard 1991; Schlesinger and Ramankutty 1994; Lall and Mann 1995) and multivariate (e.g., Allen and Smith 1994; Dettinger et al. 1995) time-domain decompositions of long climatic data series can provide important insights into the temporal organization of low-frequency climatic variability, they are best suited for broadband phenomena and less well suited for isolating more narrowband frequency-domain structure. In addition, the interpretation of significance in time-domain signals can depend quite sensitively on the assumed level of serial correlation in the data series (see Allen and Smith 1994; Elsner and Tsonis 1994). In contrast, a spectral domain approach is optimal for analyzing narrowband signals superposed on a slowly varying spectral noise background (see, e.g., Thomson 1982) and can be appropriately modified to analyze organized, broader-band frequency-domain structure. These features motivate the multivariate spectral domain SVD approach of MP94. Here we apply a generalization of that pro-

Corresponding author address: Dr. Michael E. Mann, Department of Geology and Geophysics, Kline Geology Laboratory, Yale University, P.O. Box 20819, New Haven, CT 06520-0819.

cedure to analyze spatiotemporal variability jointly between two datasets, combining a spectral domain analysis with the joint-field approach taken recently by others (Wallace et al. 1992; Xu 1993; Fraedrich et al. 1993). We apply an "evolutive" adaptation of our original procedure (see Mann et al. 1995b) that allows us to effectively identify broader-band variability associated with strongly damped unstable oscillations that are characterized by well-defined period but relatively short coherence timescales. Such a conceptual model, for example, has frequently been adopted for ENSO (e.g., Barnett 1991; Keppenne and Ghil 1992; Mann and Park 1994). Such signals may appear broadband but in fact locally may have well-defined frequency structure. The evolutive adaptation allows us to examine how frequency and amplitude characteristics of such "quasi-oscillatory" signals vary with time.

The frequency-domain SVD analysis produces a spectrum of variance within which significant narrowband peaks are determined relative to empirically determined confidence levels. We seek to isolate independent modes of variability superposed on a noise background of stochastic variability. Once identified, the SVD method can be used to reconstruct significant climatic modes in both space and time. Physical insight into the dynamical processes behind these climatic signals may be obtained by consideration of the relationship between coherent variations in the large-scale temperature and implied atmospheric circulation patterns as they evolve over a typical cycle. Simple relationships between SLP anomaly patterns, inferred surface circulation anomalies, and associated relative advective effects (warming or cooling) may suggest a largely passive response of the temperature field to circulation anomalies. Cold season warming–cooling along coastlines associated with anomalous inferred onshore–offshore circulation suggests variability in the degree of continental versus maritime influence. SST anomalies that do not reflect a passive response to atmospheric circulation anomalies may indicate underlying changes in oceanic circulation and ocean–atmosphere exchange. An analysis of the signatures provided by the joint spatial patterns thus provides insight into the underlying mechanisms of organized climate variations. Comparison with recent coupled ocean–atmosphere model simulations allows us to determine if, beyond empirical statistical inferences, there is some physical motivation for placing confidence in an apparent climatic signal.

In the first section, we describe the data used in this study. We provide a description of the analysis method in the second section. We describe the results of the analysis in the third section, focusing on the spatiotemporal patterns of statistically significant signals and discussing the similarities between the results of our empirical analysis and recent predictions of climate models. We summarize with a discussion of prospects for improved long-range climate forecasting.

2. Data

The data used consists of land, air, and sea surface temperature anomalies distributed on a $5° \times 5°$ global grid (Jones and Briffa 1992; Jones 1994) and gridded sea level pressure data on a similar but staggered $5° \times 5°$ grid in the Northern Hemisphere (Trenberth and Paulino 1980, this dataset is continually updated through the NCAR archive). We confine our spatial region to the latitude band $17.5°–72.5°$N, allowing fairly thorough spatial coverage for both fields. We use the 95-yr ($N = 1140$ months) interval 1899–1993 for which both SLP and temperature data are available. Only grid points with nearly continuous monthly sampling (very few gaps, and no single gap longer than 12 months) are used. Small gaps are filled by a simple interpolation. This should not influence our analysis, since it is confined to interannual ($\tau > 2$ year) timescales. This provides us with a set of $M = 601$ temperature grid points and $L = 792$ SLP grid points, nearly covering the subtropical to subpolar region of the Northern Hemisphere (Fig. 1), but with some spatial gaps in the temperature dataset. Possible sources of bias in the temperature data include corrections for urban warming, historical changes in data collection, and the weighting of data within grid points (see IPCC 1990; Jones and Briffa 1992). The gridded SLP, on the other hand, represent the spatial interpolation of a combination of often more sparse observations and hand-drawn analyses. These data are of somewhat questionable quality during the earliest (pre 1922) part of the century and during World War II. See Trenberth and Paulino (1980) for a detailed discussion of the quality and potential sources of bias in this data. From a spatial point of view, the data quality is poorest in high-altitude regions with strong cold-season inversions (e.g., large parts of Asia) where sea level reductions of surface measurements may be flawed. Thus, while there is potentially useful information in these data throughout the 20th century, inferences that depend heavily on the behavior of the data early in the period (such as the spatial details of long-term trends) must be caveated by potential problems in data quality. Many potential sources of bias, however, are diminished in influence by our seeking organized, dynamically consistent variations in both temperature and SLP fields. Errors that are isolated in time, for example (e.g., data problems associated with World War II) should not have a large influence in our analysis. True episodic climate behavior that may nonetheless constitute true climatic "signals" (such as surface climate perturbations due to volcanic dust loading of the stratosphere) or step-like discontinuous climatic transitions should similarly be disregarded by our search for narrowband signals or consistent time-evolving streaks of band-limited variability. Other climatic processes, such as the El Nino/Southern Oscillation (ENSO), display both episodic and periodic character (e.g., Halpert and Ropelewski
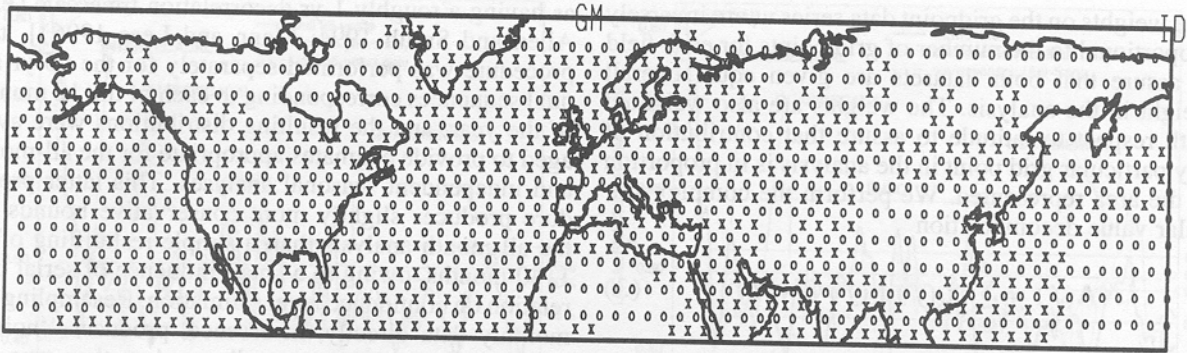
FIG. 1. Locations of grid points used in analysis, with locations of temperature data indicated by "x" and SLP data indicated by "o." The grid has latitudinal extent 15°–70°N and longitudinal extent −180° to 180°, with SLP grid points located every 5° and temperature grid points staggered 2.5°. The positions of the Greenwich meridian and international date line, as in following plots, is shown for reference.

1992) and should be reasonably, if incompletely, described by our evolutive analysis. Wavelet-based generalizations of the SVD method (Lilly and Park 1994) should be useful for isolating truly episodic variability, and for distinguishing between quasi-oscillatory and episodic characterizations of certain climate phenomena.

3. Method

We standardize for the analysis both sets of gridpoint time series by removing the long-term mean and normalizing by the long-term standard deviations on a month by month basis so that the seasonal cycle in both mean and variance is nominally removed from each gridpoint series. The variance normalization procedure favors spatially coherent processes over high-amplitude regional processes and insures that seasonality is accounted for in a consistent way. Exploiting the spatial coherence of climate signals in data series with low signal to noise ratios facilitates their identification while preserving spatial information and allowing the isolation of signals that might largely cancel in coarse spatial averaging (e.g., signals which largely involve dipole and quadrupole patterns). Analyses of (a) all-month and six-month (for simplicity), (b) cold season (October–March), and (c) warm season (April–September) data were performed separately to determine the seasonal robustness and the seasonally specific characteristics of the climatic signals under investigation. Although 6-month averaging periods were chosen for simplicity for the seasonal analyses, finer seasonal distinctions may also be worthy of investigation.

We transform the gridpoint series from the time to spectral domain using multitaper spectral analysis (Thomson 1982; Park et al. 1987). We calculate a small number (K) of independent spectral estimates of the standardized time series,

$$Y_k^{(m)}(f) = \sum_{n=1}^{N} w_n^{(k)} x_n^{(m)} e^{i2\pi fn\Delta t}, \qquad (1)$$

where $x_n^{(m)}$ is the mth standardized SLP ($m = 1 \cdots M$) or temperature ($m = M + 1, M + L$) monthly data series, Δt is the sampling interval (monthly or annual), $\{w_n^{(k)}\}_{n=1}^{N}$ is the kth member in an orthogonal sequence of K data tapers. For analysis (a) $\delta t = 1$ month, and the corresponding Nyquist frequency $f_N = 6$ cycle yr^{-1}, while for analyses (b) and (c), $\delta t = 1$ yr and $f_N = 0.5$ cycle yr^{-1}. Spectral fluctuations over a frequency width narrower than the Rayleigh frequency $f_R = 1/N\Delta t$ are generally not resolvable. The number of tapers K represents a compromise between the variance and frequency resolution of the Fourier transforms. The Slepian tapers average over a half-bandwidth of pf_R, and only the first $K = 2p - 1$ tapers are usefully resistant to spectral leakage. As in MP94, we choose a bandwidth parameter $p = 2$ and $K = 3$ tapers, which provides enough spectral degrees of freedom for a signal–noise decomposition, while allowing reasonably good frequency resolution.

At each frequency point, we form the $(M + L) \times K$ matrix

$$\mathbf{A}(f)$$

$$= \begin{bmatrix} w_1 Y_1^{(1)} & w_1 Y_2^{(1)} & \cdots & w_1 Y_K^{(1)} \\ w_2 Y_1^{(2)} & w_1 Y_2^{(2)} & \cdots & w_2 Y_K^{(2)} \\ \vdots & & & \\ w_L Y_1^{(L)} & w_L Y_2^{(L)} & \cdots & w_L Y_K^{(L)} \\ w_{L+1} Y_1^{(L+1)} & w_{L+1} Y_2^{(L+1)} & \cdots & w_{L+1} Y_K^{(L+1)} \\ w_{L+2} Y_1^{(L+2)} & w_{L+2} Y_2^{(L+2)} & \cdots & w_{L+2} Y_K^{(L+2)} \\ \vdots & & & \\ w_{L+M} Y_1^{(L+M)} & w_{L+M} Y_2^{(L+M)} & \cdots & w_{L+M} Y_K^{(L+M)} \end{bmatrix},$$

$$(2)$$

where each row is calculated from a different gridpoint time series, each column using a different data taper.

The weights on the gridpoint data series w_l are inversely proportional to the number of grid points for each field to assure that both datasets are given equal overall weight in the analysis. The weights are also weighted with respect to latitude to assure that contribution of any particular grid point in the analysis is in proportion to the area represented. We perform the complex singular value decomposition

$$\mathbf{A}(f) = \sum_{k=1}^{K} \lambda_k(f) \mathbf{u}_k(f) \otimes \mathbf{v}_k^*(f) \qquad (3)$$

into K orthonormal left-eigenvectors $\mathbf{u}_k^*$, representing empirical orthogonal functions (EOFs) in the spatial domain, and K orthonormal right-eigenvectors $\mathbf{v}_k$, representing EOFs in the spectral domain. The asterisk denotes complex conjugation, while the $\otimes$ symbol represents the tensor, or outer, product between two vectors.

The singular value $\lambda_k(f)$ scales the amplitude of the kth mode, with the singular values ordered $\lambda_1(f) \geqslant \lambda_2(f) \geqslant \cdots \geqslant 0$. The fractional variance explained by the kth mode within a given narrow-frequency band (or "local fractional variance") is given by $\lambda_k^2 / \Sigma_{j=k}^{K} \lambda_j^2$. Peaks in local fractional variance explained by the principal mode ($k = 1$) of the decomposition as a function of frequency (which we term the "local fractional variance spectrum") indicate potentially significant narrowband spatiotemporal signals in the dataset. This spectrum is determined for entire data length and as a function of time based on a moving-window version of the analysis ("evolutive" spectrum) to detect possible possible frequency, as well as amplitude modulation of processes in time, and to investigate the robustness of signals over time (see Bradley et al. 1994; Mann et al. 1995b).

Significance of peaks in the fractional variance spectrum are determined from a comparison with confidence limits obtained through a bootstrapping (Efron 1990) procedure. We assume the fairly weak condition that the noise in each individual gridpoint time series is "locally white" over the narrow bandwidth of the eigentapers. This condition amounts to the assumption that the noise component of each time series is, at any particular frequency, distributed among the $K = 3$ independent spectral estimates as it would be for white noise. Because no assumption is made about the relative variation in the overall amplitude of noise as a function of frequency, this null hypothesis is valid for time series with a fair degree of serial correlation and mildly "red" spectra (MP94). In the bootstrap procedure, the monthly temperature fields were kept spatially intact, but the 1140 months were permuted into random sequences of the same length. In each case, 1000 realizations were generated and empirical confidence levels determined from the ensemble. To guard against the potential bias of short-term serial correlation of climatic "noise" [estimated in recent analyses

as having a roughly 1-yr decorrelation timescale (e.g., Allen and Smith 1994; Mann and Lees 1996)], this procedure was performed separately for the 95-yr annual sequences corresponding to each of the 12 months of the year, and the resulting distributions were averaged to provide estimates appropriate for the all-month and independent seasonal analyses. This latter procedure produces slightly more conservative bounds for the all-month analysis than a simple reshuffling of all 1140 months, owing to a small influence of serial correlation on confidence level estimation. Resampling the monthly data directly, in essence, produces "noise" series that are more temporally random than true climate noise and leads to inflated estimates of significance. In contrast, the resampling of annually averaged (and, to a lesser extent, seasonally averaged) data provides too conservative confidence bounds because contributions from spatially correlated signals are in this case implicitly contained in the resampled series, decreasing the effective degrees of freedom in that data. The procedure we have employed, in contrast, resamples the data at an interval that exceeds the correlation timescale of the noise without averaging in low-frequency signal contributions.

The $\mathbf{v}_k$ are complex-valued K vectors and can be inverted to obtain the slowly varying envelope of the kth mode of variability near frequency f and the reconstructed time-domain signal at each grid point. In MP94, this latter step was performed in a somewhat *ad hoc* manner based on assumptions regarding the appropriate boundary constraints for the spectral to time domain inversion. In the present study, we have removed this subjective step by choosing, among all possible weighted combinations of "minimum norm" and "minimum roughness" time-domain solutions (see Park and Maasch 1993; MP94), the combination that maximizes the explained variance in the multivariate dataset. For the fixed frequency peaks (secular, interdecadal, and quasi-decadal), the time reconstructions are performed using the procedure outlined in MP94, with this revised inversion method. For the time-evolving signals (as determined in the evolutive analysis), we perform a multivariate projection filtering [a variant on the univariate procedure described by Thomson (1995)] in which the contributions of signal estimates at a particular point in time are averaged from the moving window of the evolutive analysis. The carrier frequency in the reconstruction, potentially drifting in time, is estimated from the evolutive SVD spectrum.

The $\mathbf{u}_k$ are complex-valued $(M + L)$ vectors that determine the relative pattern in phase and amplitude of the gridpoint temperature and SLP variations for the kth mode of variability. The spatial patterns are thus reconstructed by nonnormalizing the $\mathbf{u}_k$ by the gridpoint standard deviations. These patterns describe the evolving spatial pattern of a signal over a typical cycle. Our analysis describes equally well spatially standing or propagating patterns, with the exception of secular
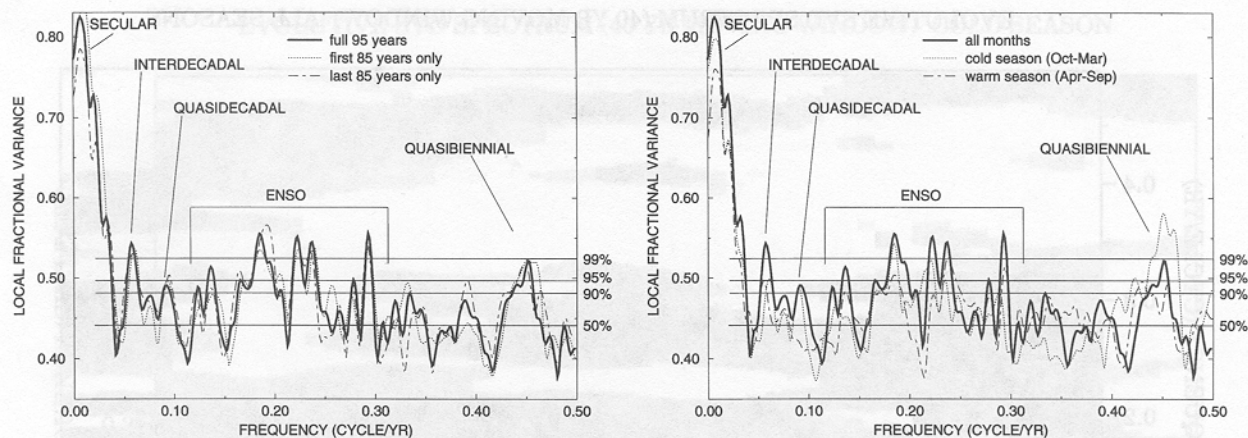
FIG. 2. (a) SVD spectrum (relative variance explained by the first eigenvalue of the SVD as a function of frequency). Horizontal dashed lines denote median (50%), the Monte Carlo simulations (confidence limits within the secular band $f < 0.02$ cpy are somewhat higher—see MP94). (b) SVD spectrum based for all-month and cold- and warm-season analyses. The confidence levels shown are for the all-month analyses with significance levels slightly different for the cold ($\sim +0.01$ for each) and warm (~ -0.01 for each) season analyses.

variations for which only the relative sign of variations can be determined. This approach thus provides a signal description that is similar to that of complex principal component analysis or "complex harmonic PCA" (see, e.g., Barnett 1983; Trenberth and Shin 1984; Barnett 1991; Preisendorfer 1988), but seeks to generalize upon such an approach by using a *frequency domain* SVD to isolate modes of band-limited variability that are described by a single spatially correlated modulating time envelope. In the case of the "evolutively" determined signals, the relative spatial patterns (in both amplitude and phase) vary somewhat over time, consistent with the possible nonstationarity of the associated climate process [see, for example, the discussion of secular changes in the characteristic effect of ENSO on precipitation patterns in certain regions in Ropelewski and Halpert (1987)]. For simplicity, the average spatial pattern over time is shown in such cases.

4. Results

a. Multivariate SVD spectra

Similar to the analysis of globally distributed temperature data in MP94, the joint-mode fractional variance spectrum based on the full 95 years (1140 months) of data (Fig. 2a) yields significant variance peaks on the quasibiennial (2.1–2.2 year) timescale, within the 3–7 yr ENSO period band, on "quasidecadal" (10–11-yr period) and "interdecadal" (16–18-yr period) timescales. Two significant modes are identified within the secular band that averages variability on timescales $\tau > N\Delta t/2 = 48$ yr. It is worth noting that while the spectra averaged over the contributions of the K eigentapers have a relatively broad bandwidth of $\Delta f \approx 0.04$ cycles per year (cpy), the

SVD spectrum provides potentially greater frequency resolution (with the fundamental limit provided by the Rayleigh resolution $f_R \approx 0.01$) through weighted combinations of the independent eigenspectra. A somewhat restricted sensitivity test (see Fig. 2a) in which we use 85-yr data subsegments long enough to resolve the secular and relatively closely spaced quasidecadal and interdecadal peaks demonstrates relative stability in the significance of the dominant peaks evident in the analysis of the full 95 years of data. For the interannual signals, a more liberal sensitivity test can be performed, as described below.

Comparison of SVD spectra for all-, warm-, and cold-season data (Fig. 2b) suggest that secular and interdecadal signals are seasonally robust, although the spatial signature of these signals, mostly in middle and high latitudes, are shown below to display seasonally specific features. The interdecadal signal appears to derive its strong ($>99\%$) significance in the all-season analysis from more moderate but consistent levels of significance during distinct seasons. The ENSO-band variance peaks show some distinct differences between the all-seasons and seasonal analyses. The quasidecadal signal appears as a distinctly cold-season phenomenon. The quasibiennial signal is significant during both independent seasons but is clearly stronger during the cold season (we have checked, through analysis of synthetic examples, that no significant bias is introduced by the proximity to f_N for the seasonal analyses). It is possible that a seasonally persistent signal is only *detectable* above noise at certain times in our analysis. For example a low-frequency carrier signal in tropical SST may only lead to a larger-scale expression during the winter season when high-amplitude extratropical circulation anomalies are induced. An independent analysis of the spatial and temporal patterns for both seasons provides insight into such issues.

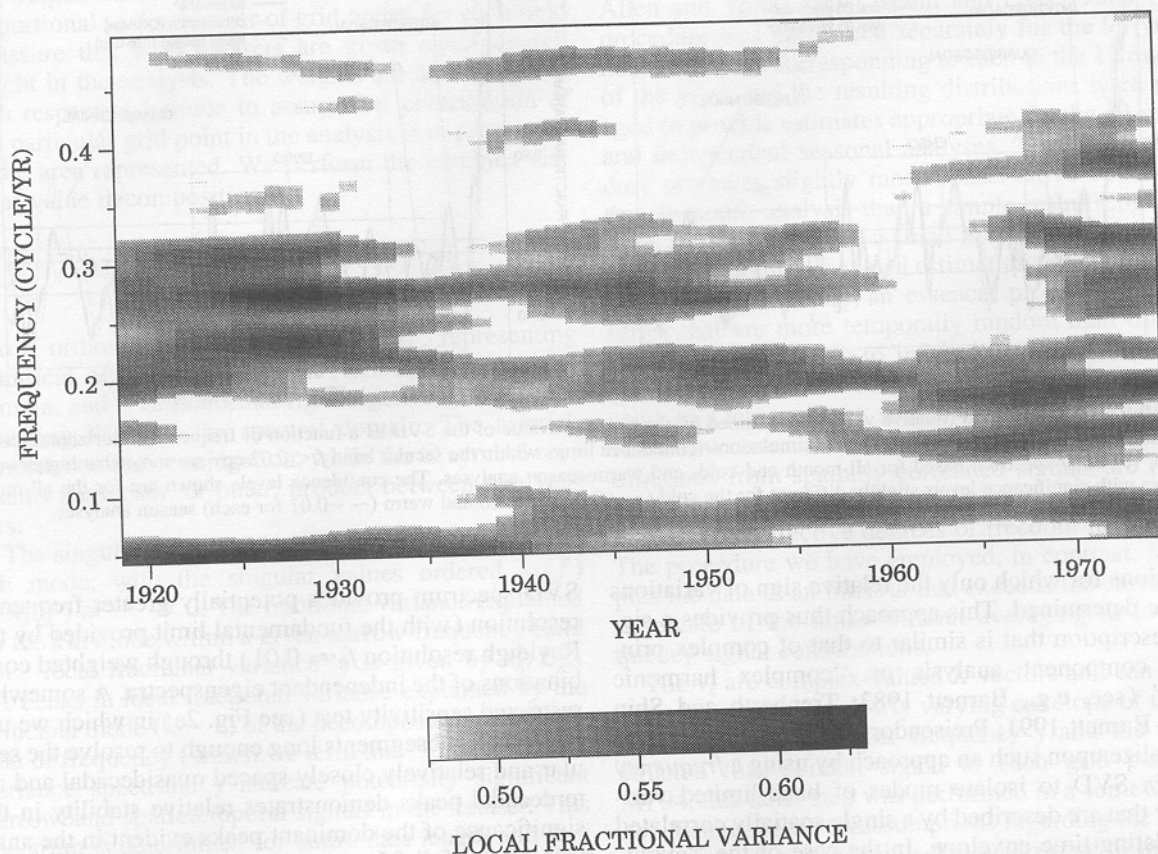## EVOLUTIVE SVD SPECTRUM (40 YR MOVING WINDOW) ALL SEASONS

FIG. 3. Evolutive SVD spectrum based on performing the SVD analysis in a moving 40-yr window for (a) all seasons, (b) cold season, and (c) warm season. The amplitude of the spectrum as a function of time (center of moving window) and frequency is shown with the indicated grayscale, with confidence levels associated with the values given in Fig. 2. Only the frequency range resolvable from zero frequency ($f > 0.05$ for the tapers of bandwidth parameter $p = 2$ and $p = 40$ yr window width) is shown.

We determined the evolutive SVD spectrum (Fig. 3) using an $N = 40$ yr moving window through the dataset (see Mann et al. 1995b). This choice of window width admits a frequency resolution 0.10 cycle yr^{-1} so that the quasidecadal and interdecadal peaks in Fig. 2 are not resolved, and only periods shorter than 20 years can be separated from a secular trend. The relative stability of interannual timescale signals, and the potential time-dependence of the amplitude and frequency characteristics, can however be effectively tested by this latter analysis. Employing a 40-yr window with $K = 3$ spectral degrees of freedom allows roughly for the existence of one phase discontinuity per 13 years. Thus, low-frequency (5–7-yr timescale) ENSO variability is assumed to maintain coherence (and vary in amplitude) over two to three "cycles." In contrast, the quasibiennial oscillation is modeled as being phase coherent (and varying in amplitude) over roughly five cycles. Thus, for the QBO signal reconstruction (see below), we employ a somewhat shorter 20-yr window. In the all-months analysis (Figure 3a), there is clear evidence

of organized frequency-domain structure within the ENSO band, with two dominant bands of variability clustered around 3–4 yr and 5–7 yr period bands that exhibit appreciable frequency and amplitude modulation. This behavior is *approximated* in the full window analysis by amplitude-modulated statistically significant quasi-oscillatory components centered near 3-, 4-, 5-, and 7-yr periods. While a more complicated behavior is evident in the evolutive analysis, the degree of frequency-domain organization belies a simple *episodic* picture and reinforces the utility of a frequency-domain analysis of ENSO variability. The cold (Fig. 3b) and warm season (Fig. 3c) only analyses show streaks of variance within these two same dominant bands, but the relative lack of frequency domain structure evident in the latter analyses implies a signal that is not simply phase-locked to the annual cycle. Nonetheless, the separate cold and warm seasonal signal reconstructions are essential to understanding the relationship between tropical and extratropical expressions of the signal. The seasonal analyses substantiate the

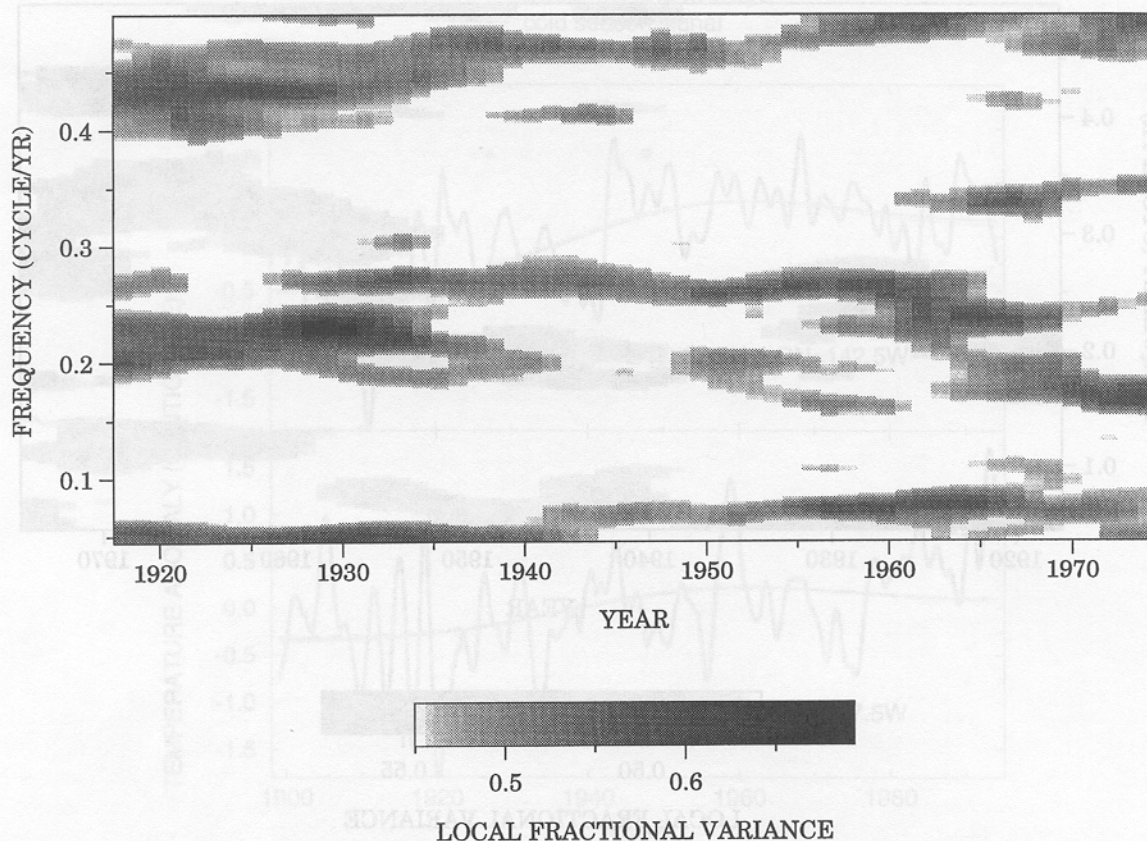EVOLUTIVE SVD SPECTRUM (40 YR MOVING WINDOW) COLD SEASON

FIG. 3. (Continued)

cold-season dominance of the QBO signal and reveal a drifting trend toward higher frequency.

b. Secular modes

The primary secular mode (Fig. 4), accounting for 77% of the low-frequency variance in the joint SLP-temperature dataset, is associated with a warming trend (see Ghil and Vautard 1991; MP94) that displays most rapid increase between 1920 and 1940 and slight cooling after 1950. The warming is coherent with changes in SLP that imply altered patterns of surface atmospheric circulation. The continued acceleration of global warming in certain regions through the 1990s is not associated, in the context of our study, with the long-term global secular warming trend, but may rather represent an acceleration in global warming associated with an apparent nonstationary shift to sustained ENSO-like global climate patterns (see Trenberth and Hoar 1995). This is highlighted by the fact that a marked positive departure from the low-frequency global warming trend is found in the far eastern tropical Pacific (within the reach of positive El Niño SST anomalies) but not in the more central subtropical Pa-

cific (Fig. 4a). Much of the warmth of the 1980s (but *not* the 1990s) is, in contrast, explained by interdecadal fluctuations (see below).

The pattern of secular warming is largely robust between cold (Fig. 4b) and warm season (Fig. 4c), although certain regions show a marked seasonal-dependence. For example, secular warming in eastern Asia and the North Atlantic is present only during the cold season, which might be related to winter land and sea-ice albedo effects. In the southeastern United States, the presence of cold-season cooling and warm-season warming might be related to an anomalous circulation pattern [e.g., a troughlike trend over North America discussed elsewhere by Mann et al. (1995a)] that favor a more continental influence in the region. Over the North Atlantic, a winter season north–south trend toward a reverse North Atlantic Oscillation (NAO)-like SLP dipole pattern [Deser and Blackmon (1993), see also Barnston and Livezey (1987) for a discussion of this and other atmospheric circulation anomaly patterns discussed subsequently in the text] could explain some of the asymmetry in warming along the western and eastern margins of the North Atlantic basin, although changes in heat transport by the Gulf Stream have also

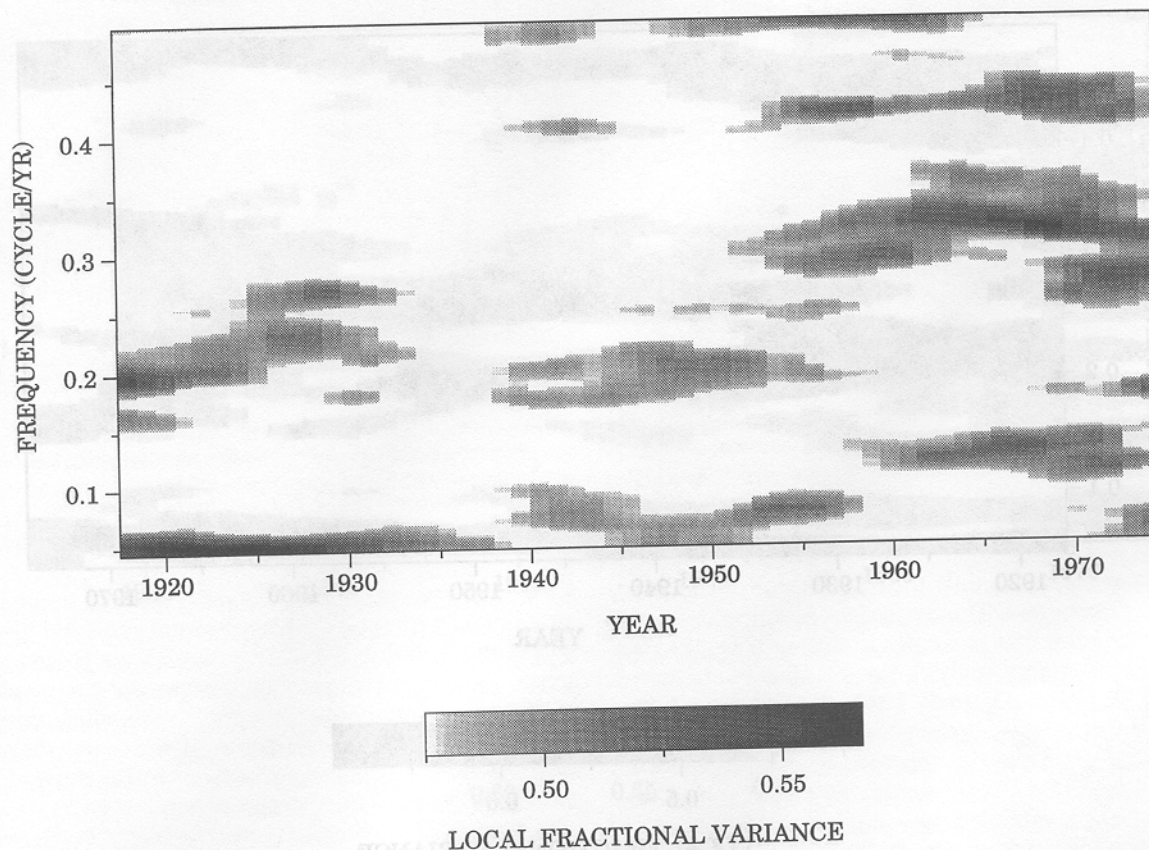## EVOLUTIVE SVD SPECTRUM (40 YR MOVING WINDOW) WARM SEASON

FIG. 3. (Continued)

been speculated (Deser and Blackmon 1993). Quali-tatively similar, if not identical, circulation anomalies to those noted above have been variously observed in GCM simulations of the climatic response to green-house gas forcing (IPCC, chapter 5, 1990; Oglesby and Saltzman 1992; Marshall et al. 1995). Other circulation anomalies are suggested, but some of the observed sig-nal may be spurious. The questionable quality of the earlier SLP data and potential problems with reduction of pressure measurements to sea level in certain regions (e.g., cold-season central Asia) demand a cautious in-terpretation. The sharp anomalous SLP anomaly fea-tures near northern Japan–Sea of Okhotsk correspond to the behavior of a small number of grid points and could be spurious.

The secondary secular mode (Fig. 5) accounts for a lesser, but nonetheless significant (21%), share of the zero-frequency centered variance. This signal is asso-ciated with a pattern of high-amplitude warming and subsequent cooling in the North Atlantic, describing a roughly 75-yr timescale standing "oscillation" (Fig. 5a), consistent with other recent studies of long-term (Kushnir 1994; Schlesinger and Ramankutty 1994; MP94—the timescale is better constrained in the pres-

ent study by the improved time-domain inversion pro-cedure) trends in the North Atlantic, as well as evi-dence of persistent century-scale oscillations over the last 500 years detected by a spatiotemporal analysis of globally distributed temperature proxy records (Mann et al. 1995b). MP94 argued for a relationship with in-stabilities in the thermohaline circulation based on the global pattern of surface temperature anomalies that are out of phase between the North Atlantic and remaining World Ocean. Delworth et al. (1993, henceforth DEL93) have demonstrated that such century timescale (more precisely, 40–60-yr period) oscillatory behavior can arise from instabilities in the thermohaline circu-lation based on 1000-yr coupled ocean–atmosphere model simulation. In that study, a pattern of anoma-lously warm SSTs in the midlatitude and polar North Atlantic and slight cold anomalies in parts of tropical–subtropical North Atlantic were associated with the en-hanced thermohaline circulation phase of the oscilla-tion. Enhanced thermohaline circulation was in turn as-sociated with a pattern of negative high-latitude and positive low-latitude SLP anomalies over the North At-lantic, which appear to be a result of, rather than an intrinsic component to, the underlying instability. The
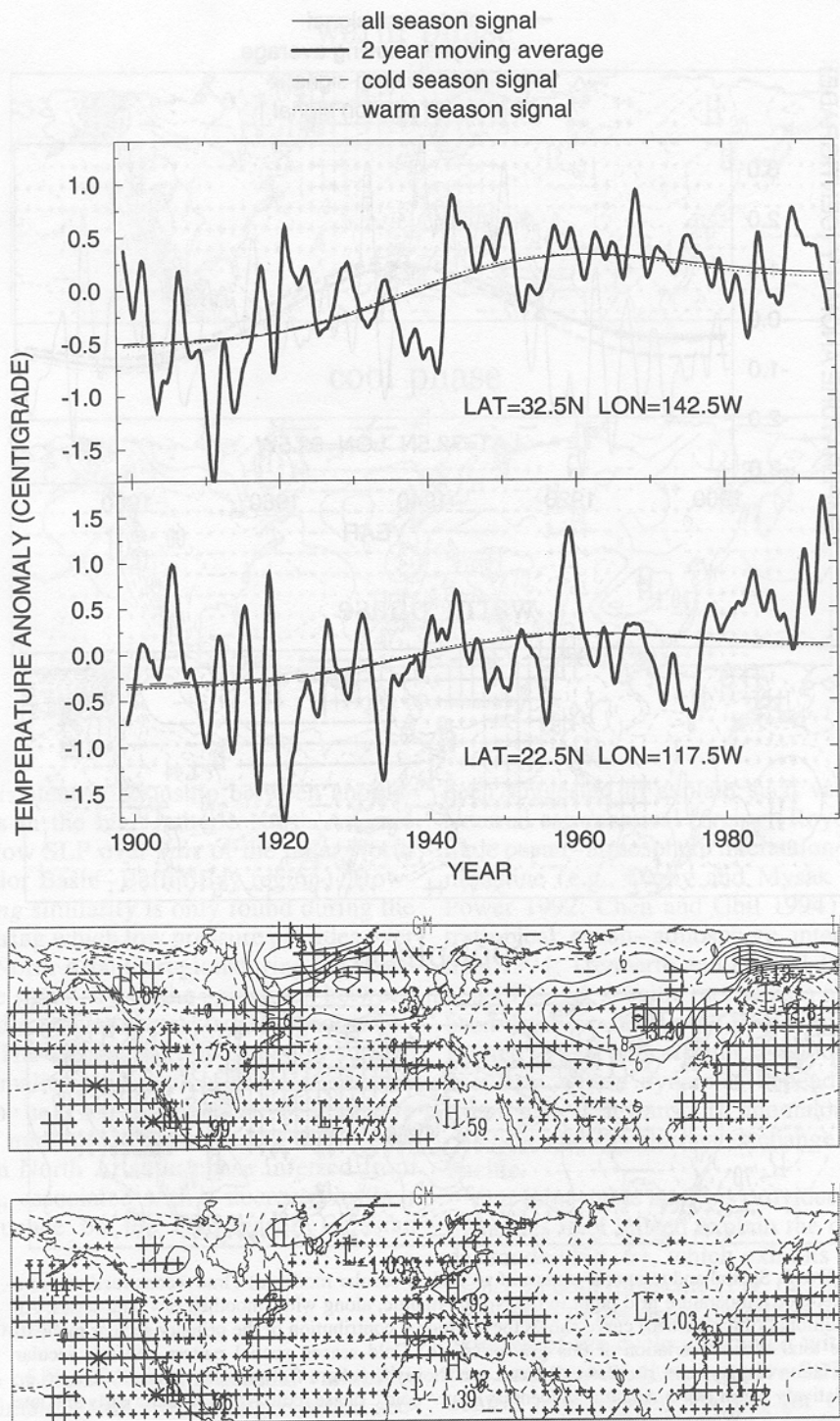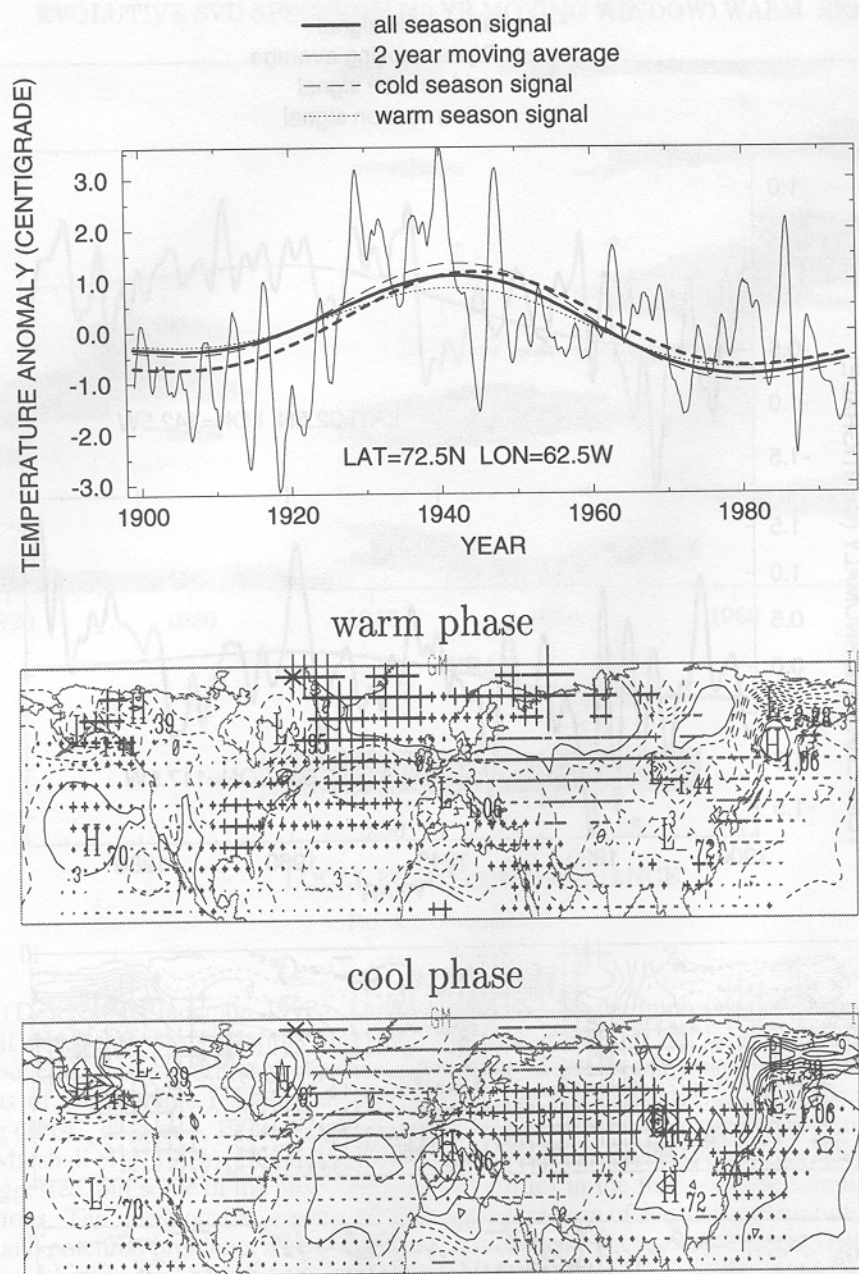
FIG. 4. Spatial and temporal pattern of primary secular mode. (a) Time reconstructions for at reference temperature grid points in the (i) central subtropical and (ii) eastern tropical Pacific, along with smoothed interannual (24-point cosine tapered) moving averages of the raw gridpoint data. (b) Cold season spatial pattern. As in all similar subsequent plots, temperature anomalies are shown with ''+'' (''−'') symbols with magnitudes proportional to the size of the associated warm (cold) anomaly. SLP patterns are contoured in units of millibars (mb). The two reference grid points of (a) are shown with ''X'' symbols and provide an absolute scale for the temperature anomaly pattern. (c) Warm season spatial pattern.

FIG. 5. Spatial and temporal pattern of secondary secular mode. (a) Time reconstructions for a reference temperature grid point in the North Atlantic, along with smoothed raw data series. An additional (thick dashed) curve shows the additional contribution of the primary secular mode to the total secular variation at this grid point. (b) Cold season spatial pattern. As this secular variation displays an "oscillatory" trend, we show the pattern for both the "warm" phase (i.e., relatively warm North Atlantic midcentury) and "cold" phase (cold North Atlantic early and late century). (c) Warm season spatial pattern.

opposite features were associated with the weakened state of thermohaline circulation.

We find additional, though not conclusive, support for such a coupled pattern in association with the observed century-scale signal. The North Atlantic regional features of the signal confirm the earlier analysis by Kushnir (1994), who observed some similarity with the simulation results of DEL93. We find a pattern of surface temperature variability in the North Atlantic, robust from cold (Fig. 5b) to warm (Fig. 5c) season, that resembles the surface temperature patterns of the DEL93 signal. Furthermore, consistent with DEL93,
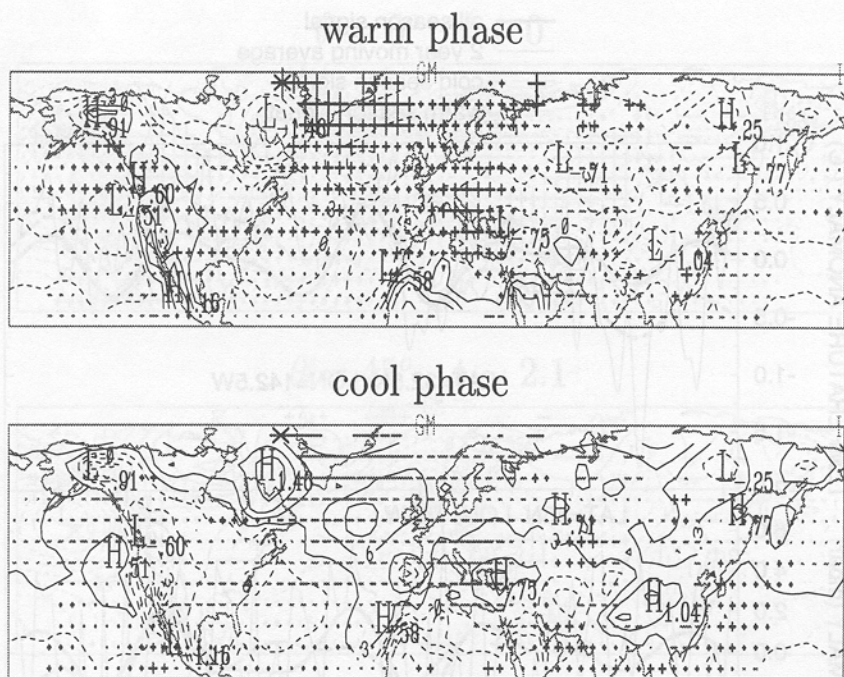
warm phase

cool phase

FIG. 5. (*Continued*)

we do find a persistent relationship between anomalous warm SSTs in the high-latitude North Atlantic and anomalous low SLP over *part* of the polar North Atlantic (Labrador Basin–Baffin Bay region). However, a *convincing* similarity is only found during the warm season, during which low pressure presides over the entire polar North Atlantic region during the warm SST phase of the signal. Thus, the agreement between the observed and modeled century-scale signal is imperfect at best. The substantial opposite-sign surface temperature anomalies over much of Eurasia (see also MP94) during the cold season appears to be related to a breakdown of midlatitude westerlies in that region during the warm North Atlantic phase inferred from the SLP pattern, associated with a decrease in their moderating influence on the cold-season Eurasian climate.

c. Interdecadal mode

The existence of significant interdecadal variability in the surface climate, distinct from longer-period secular variations, has been established in both historical observations (Ghil and Vautard 1991; Trenberth 1990; Mann and Park 1993; Royer 1993; Tanimoto et al. 1993; Trenberth and Hurrell 1994; MP94; Unal and Ghil 1995) and through coupled ocean–atmosphere modeling studies (Mysak and Power 1992; Barnett et al. 1992; Darby and Mysak 1993; Graham 1994; von Storch 1994; Latif and Barnett 1994; Miller et al. 1994; Chen and Ghil 1995). A variety of mechanisms have

been suggested to explain such variability, including external astronomical forcing (Royer 1993), high-latitude ocean–atmosphere interaction involving the thermohaline (e.g., Darby and Mysak 1993; Mysak and Power 1992; Chen and Ghil 1994), and unstable extratropical ocean–atmosphere interaction (e.g., Graham 1994; Trenberth and Hurrell 1994; Latif and Barnett 1994). A specific mechanism of the latter type has been demonstrated in the modeling study of Latif and Barnett (1994, henceforth LB94), describing a delayed oscillator whose dynamics depend on feedbacks between gyre heat transport, anomalous atmospheric circulation, and air–sea heat exchange in the extratropical Pacific.

Our joint-mode analysis provides evidence that such dynamics may indeed explain the observed interdecadal mode (Fig. 6), which exhibits remarkable resemblance in both timescale (Fig. 6a) and spatial evolution (Fig. 6bc) to the signal described by LB94. During the extreme of the cycle associated with anomalous negative heat content (i.e., negative SST anomalies) in the central extratropical Pacific, for example, one finds anomalous positive SSTs in the lower-latitude North Pacific (and thus an increased latitudinal SST gradient), accompanying anomalous low wintertime SLP over the North Pacific, and inferred strengthening of midlatitude westerlies (Fig. 6b). At the other extreme of the cycle, these patterns are reversed. This relationship is argued by LB94 to reflect a sequence of positive and negative feedbacks whereby the meridional SST gradient modifies the planetary wave structure and thus
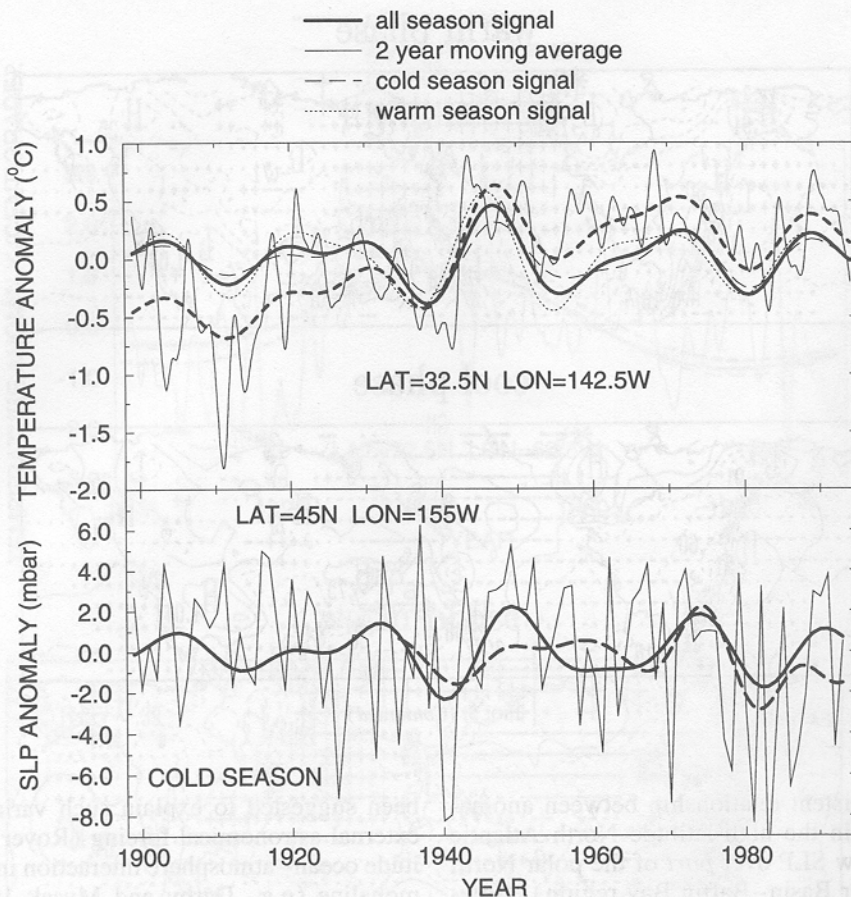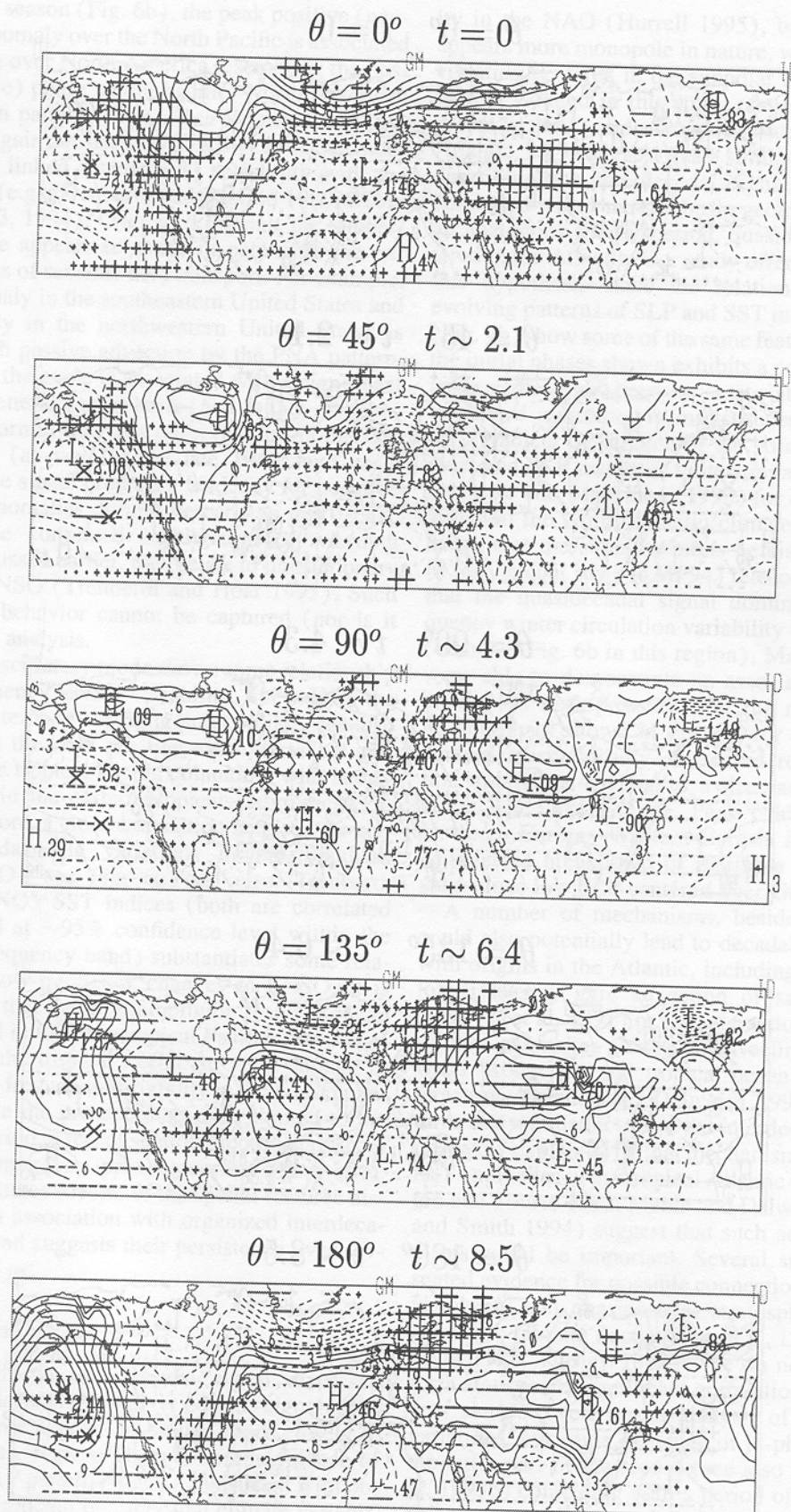
FIG. 6. Spatial and temporal pattern of interdecadal mode. (a) Time reconstruction for (i) reference subtropical east-central Pacific temperature grid point and (ii) reference midlatitude central Pacific SLP grid point (cold season) along with the smoothed raw data series. The thick dashed line in (i) indicates the sum of the secular warming trend (see Fig. 4a) and interdecadal mode. The thick long-dashed line in (ii) shows the interdecadal and longer-term (lowpassed with a notch at 10-yr period) variations in the SOI (scaled by a factor of 3 in mb) since continuous data is available, demonstrating an in-phase relationship of decadal-scale variations with the projection of the interdecadal signal onto cold-season winter North Pacific SLP. (b) Cold-season spatial pattern shown at progressive intervals, spanning one-half of a complete (~17 year) cycle. The initial snapshot corresponds to peak winter trough (and peak negative SST anomalies) in the central midlatitude North Pacific, while the final snapshot corresponds to the opposite conditions that obtain one-half cycle (i.e., ~8.5 years) later. The absolute timing of relative phases of the pattern are defined by the reference SLP or temperature series. (c) Warm-season spatial pattern.

the latitudinal gradient in windstress curl, altering the poleward heat transport by the North Pacific gyre and thus, in turn, the SSTs themselves. The roughly 20-yr timescale of an oscillatory cycle is attributed to the intrinsic spinup timescale of the North Pacific gyre, with the adjustment in gyre heat transport lagging wind stress changes by several years, thus providing feedbacks that support oscillatory behavior. The warm-season expression of the signal (Fig. 6c) emphasizes the seasonal persistence (and consistency) of the SST anomalies in the Pacific that appear to lead, during the cold season only, to high-amplitude extratropical circulation anomalies. One notable exception is an implied strengthening and weakening

of the Asian monsoonal pattern associated with seasonally opposite SLP variations over central Asia. While some strong similarity is found with the simulations of LB94, there are notable discrepancies as well. For example, the interdecadal pattern of LB94 is strongest over the western North Pacific where the model SST gradient is largest, in contrast to the eastern North Pacific centered pattern isolated in our analysis. Furthermore, high amplitude variability in the Atlantic region and elsewhere suggests either strong downstream teleconnections or perhaps coupling with Atlantic basin processes that are not observed in LB94. Such complications are discussed further in section 4d.
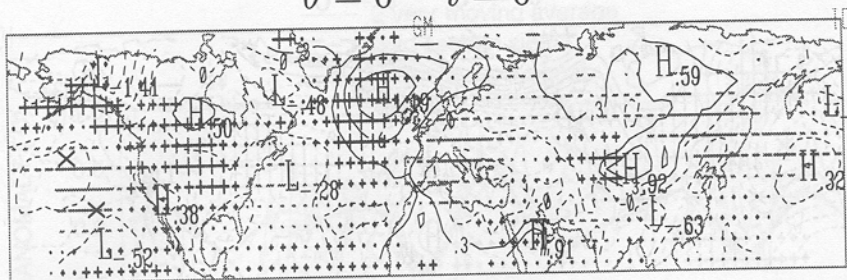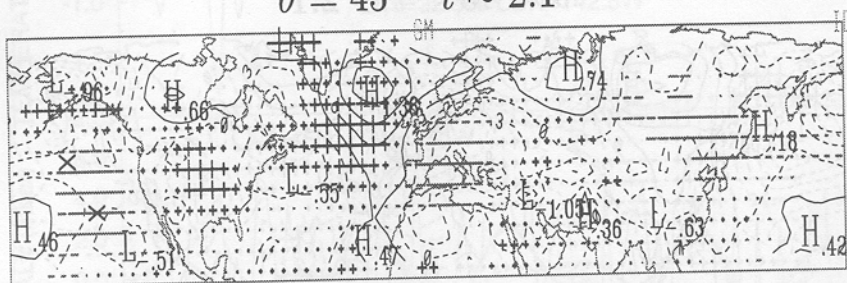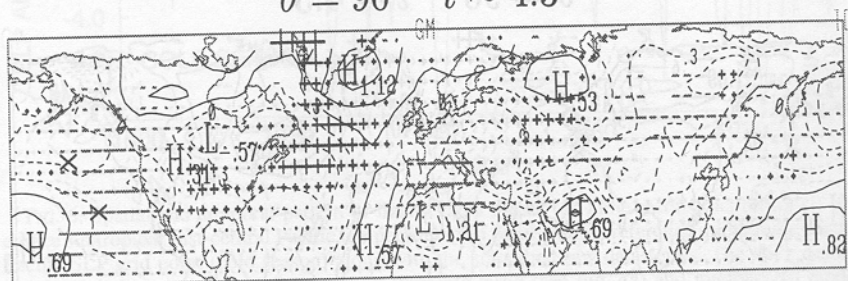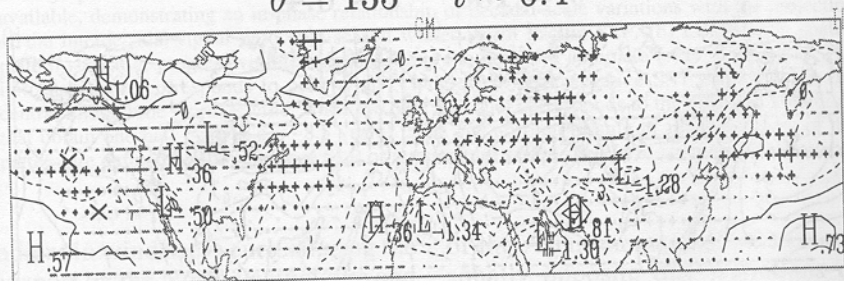
$\theta = 0^{o}$ $t = 0$

$\theta = 45^{o}$ $t \sim 2.1$

$\theta = 90^{o}$ $t \sim 4.3$

$\theta = 135^{o}$ $t \sim 6.4$

$\theta = 180^{o}$ $t \sim 8.5$

FIG. 6. (*Continued*)

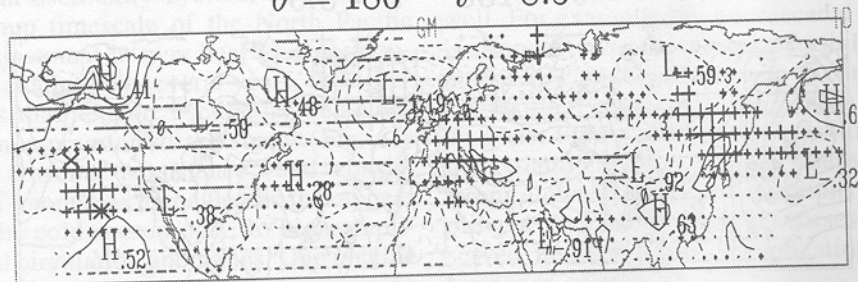$$\theta = 0^o \quad t = 0$$

$$\theta = 45^o \quad t \sim 2.1$$

$$\theta = 90^o \quad t \sim 4.3$$

$$\theta = 135^o \quad t \sim 6.4$$

$$\theta = 180^o \quad t \sim 8.5$$

Fig. 6. (Continued)

In the cold season (Fig. 6b), the peak positive (negative) SLP anomaly over the North Pacific is associated with a pattern over North America resembling the positive (negative) phase of the Pacific–North American teleconnection pattern (PNA—see Barnston and Livezey 1987), again consistent with LB94 and other studies that have linked interdecadal variability with the PNA pattern (e.g., Trenberth and Paolino 1980; Mann and Park 1993, 1994). Over land regions, the temperature response appears to result in part from the expected patterns of sensible heat transport. For example, the cold anomaly in the southeastern United States and warm anomaly in the northwestern United States is consistent with passive advection by the PNA pattern. This phase of the cycle is associated with a significant share of the general hemispheric (and in fact global—see MP94) warmth that was observed during the mid to late 1980s (as well as the late 1940s and early 1970s), but the signal projects a tendency for negative temperature anomalies during the early to mid 1990s, counter to the continued acceleration of warming which, as discussed earlier, may relate to nonstationary behavior in ENSO (Trenberth and Hoar 1995). Such nonstationary behavior cannot be captured (nor is it sought) in our analysis.

This quasi-oscillatory mode shows some relationship with low-frequency ENSO variability, not only in the ENSO-like patterns of warming and cooling (see also MP94), but in the mild positive east–west SLP gradient across the tropical Pacific coinciding with anomalous warmth in the eastern tropical–subtropical Pacific. Furthermore, a close association between the signal and decadal-scale variations in the Southern Oscillation (SO—see Fig. 6a, and also, Trenberth 1990) and NINO3 SST indices (both are correlated with our signal at ~95% confidence level within the interdecadal frequency band) substantiates some relationship with low-frequency changes in ENSO. It is quite plausible that the high-amplitude features of the signal, centered in the extratropical Pacific, may nonetheless impact the tropical Pacific strongly enough to force weak low-frequency variability in the ENSO phenomenon. While the present analysis is limited to the instrumental period, a recent spatiotemporal analysis of longer-term temperature proxy records (Mann et al. 1995b) substantiates several of the spatial features discussed above in association with organized interdecadal variability and suggests their persistence over several centuries.

d. Quasi-decadal mode

In contrast to the interdecadal signal discussed above, a quasi-decadal (10–11-yr period) signal has a spatial pattern that appears to be tied more closely to the North Atlantic region. There is some evidence of an NAO-type SLP pattern (Fig. 7), consistent with observations of significant quasidecadal climate variability in the NAO (Hurrell 1995), but the SLP pattern appears more monopole in nature, with high-amplitude variation centered in the subpolar North Atlantic. The pattern isolated in this study may represent a combination of NAO and monopole structures in the North Atlantic. LB94 suggest that a similar mechanism to that describing the interdecadal signal discussed above, combined with a narrow basin geometry, could lead to an analogous shorter-period, quasidecadal signal centered in the Atlantic. Our study offers some support for this hypothesis since the relationship between the evolving patterns of SLP and SST in the North Atlantic (Fig. 7b) show some of the same features. For example, the initial phases shown exhibits a consistent pattern of anomalous high pressure associated with inferred weakened westerlies in midlatitudes and a decreased SST gradient over much of the Atlantic. The temperature and SLP pattern is quite similar to that identified by Deser and Blackmon (1993) for quasidecadal variations in the North Atlantic climate, but there is evidence that the signal exhibits hemisphere-scale (and, in fact, global scale—MP94) teleconnections. Noting that the quasidecadal signal dominates the low-frequency winter circulation variability in the Great Basin (compare Fig. 6b in this region), Mann et al. (1995a) were able to demonstrate an association between the anomalous high pressure over the region during the middle phase shown in Fig. 8b, for example, and decreased storm activity–decreased regional precipitation anomalies leading to a decreasing trend in the Great Salt Lake volume. Peak cold conditions over Northern Europe–Western Eurasia is consistent with an inferred breakdown of maritime influence due to anomalous low SLP centered over Great Britain.

A number of mechanisms, besides that of LB94, could also potentially lead to decadal-scale variability with origins in the Atlantic, including the influence of low-frequency gyre advection of salinity anomalies (Weaver et al. 1991) or the interaction of thermal and salinity anomalies (Yang and Neelin 1993) on deep water production and tropical ocean–atmosphere interactions (Mehta and Delworth 1995). Certain features that are distinct from the interdecadal pattern and not easily explained by that mechanism, including large SST anomalies in the tropical Atlantic (see also Houghton and Tourre 1992; Mehta and Delworth 1995; Allen and Smith 1994) suggest that such additional mechanisms could be important. Several studies have presented evidence for possible connections between solar variability and quasidecadal stratospheric–upper-tropospheric climate fluctuations (e.g., Labitzke and van Loon 1988; Tinsley 1988). We do not find evidence for a statistically significant correlation with the ~11-year sunspot cycle in our analysis of surface climate variations, but some evidence of in-phase behavior in the latter part of the record (see also MP94; Mann et al. 1995b) coinciding with a period of high amplitude solar cycle variations might be argued for. The argu-
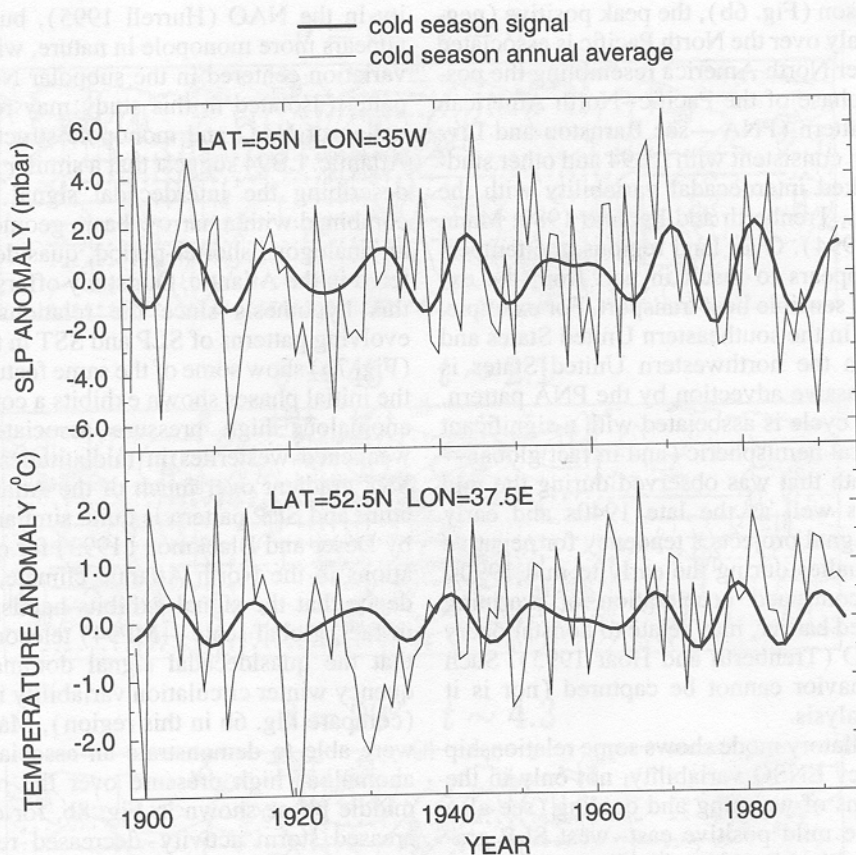
FIG. 7. Spatial and temporal pattern of quasidecadal mode. (a) Time reconstruction for (i) reference midlatitude–subpolar North Pacific SLP grid point (cold season) and (ii) similar latitude western Soviet temperature grid point. Note the 90° phase lag between the two variations, as expected from the discussion in the text. (b) Cold-season spatial pattern spanning one-half of complete (~11 year) cycle. The initial snapshot corresponds to the peak positive winter SLP anomaly over the North Atlantic, and the final snapshot to the opposite conditions one-half cycle (~5.4 year) later.

ment that internal decadal-scale variability could resonate with such external forcing, if high enough amplitude, cannot be ruled out.

The cold-season nature of the quasidecadal signal seems to relate to the fact that it is not strongly associated with any seasonally persistent tropical variability but, rather, seems to force winter SST variability in certain regions of the Tropics largely through anomalous southerly or northerly advection by cold-season midlatitude SLP anomalies. Furthermore, no significant connection is found with ENSO. The relatively weak nature of this signal, and the lack of a truly convincing spectral gap (see Fig. 2) between the interdecadal and quasidecadal peaks, as well as some apparent coupling of processes, particularly evident in the Pacific, nonetheless limits the degree of confidence that should be placed in this signal. With the short duration of instrumental data available, it is difficult to adequately distinguish between the statistical models of two distinct peaks associated with distinct but analogous mecha-

nisms in the Atlantic and Pacific, and a single broaderband, coupled basin, decadal-scale signal. It is clear that this variability is far from being well understood. Independent analyses of the variations in independent Atlantic and Pacific basin subregions may better clarify the nature of the observed decadal-scale climate signal(s).

e. ENSO signal

Previous analyses of global precipitation patterns (Ropelewski and Halpert 1987), continental precipitation and temperature variability (Bradley et al. 1987) and global surface temperature patterns (Halpert and Ropelewski 1992) associated with ENSO events, frequency-domain studies of tropical–subtropical SST and oceanic SLP (Barnett 1991), and globally distributed surface temperature data (Mann and Park 1993; MP94) have provided complementary insights into the global ENSO phenomenon. Nonetheless, the large-
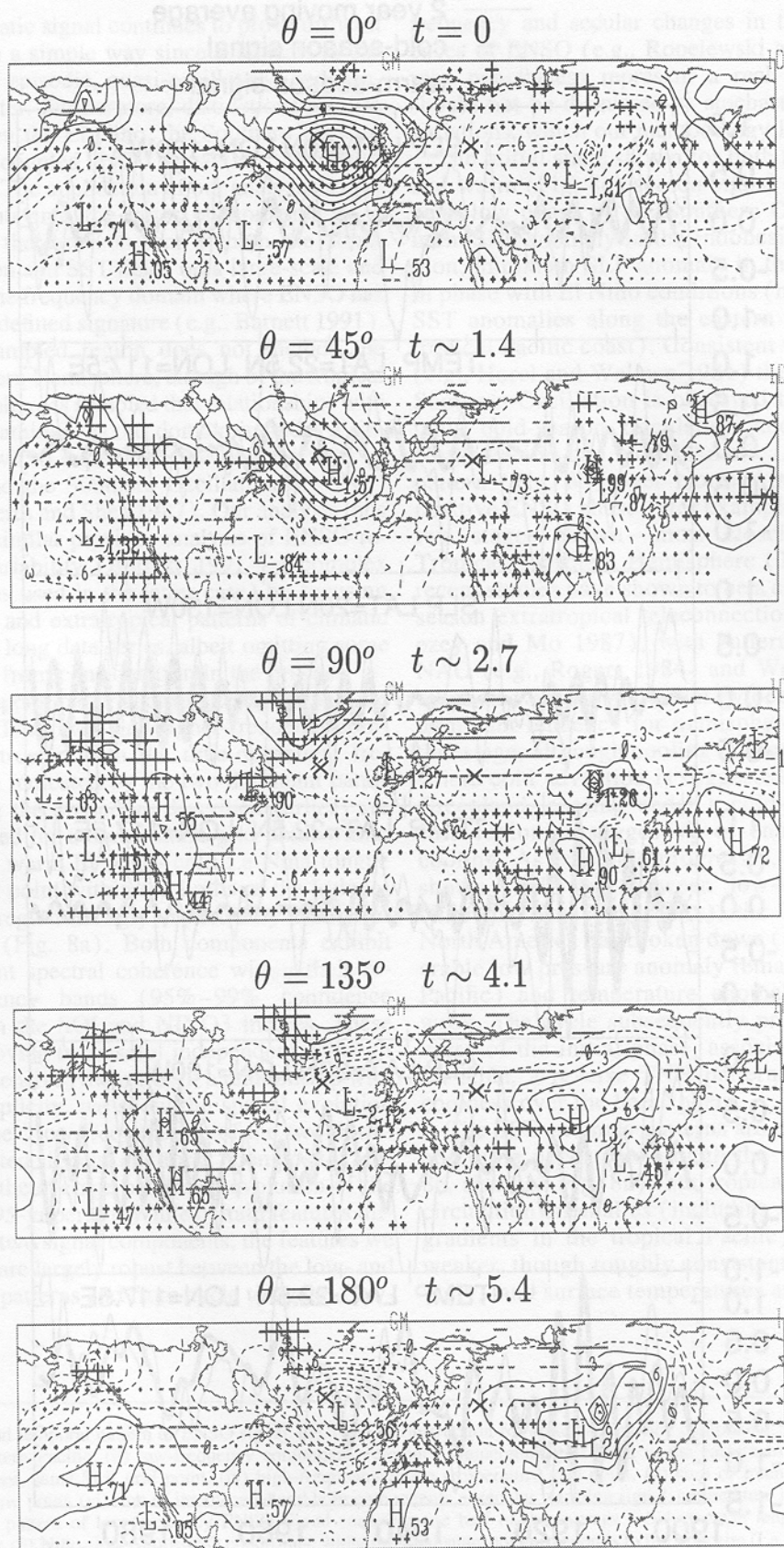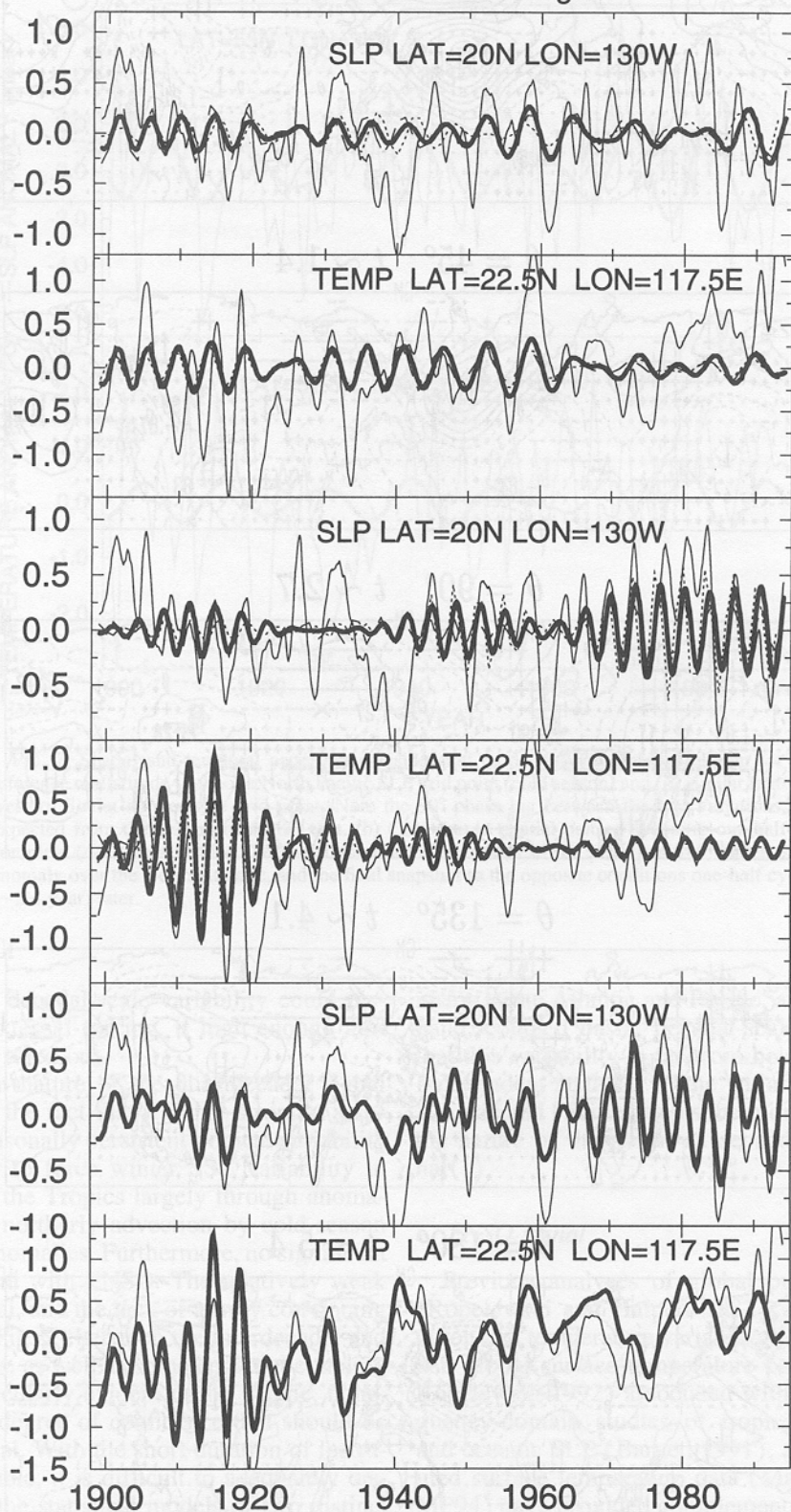
FIG. 7. (Continued)

all season signal
2 year moving average
cold-season signal
warm-season signal

SLP LAT=20N LON=130W

TEMP LAT=22.5N LON=117.5E

SLP LAT=20N LON=130W

TEMP LAT=22.5N LON=117.5E

SLP LAT=20N LON=130W

TEMP LAT=22.5N LON=117.5E

1900   1920   1940   1960   1980

scale ENSO climatic signal continues to prove difficult to characterize in a simple way since it appears to exhibit evidence of episodic, quasi-oscillatory, and non-stationary character. Furthermore, distinctions need to be drawn between the El Niño, the Southern Oscillation, and the true coupled ENSO signal (e.g., Trenberth and Hoar 1995). The application of our analysis is thus useful for insights into the latter phenomenon as it seeks variations that are coherent in both the atmospheric circulation and SST fields on a large-scale and is performed in the frequency domain where ENSO has a relatively well-defined signature (e.g., Barnett 1991). Although our sampled region does not include the equator or Southern Hemisphere, enough of the tropical Northern Hemisphere is sampled that relationships with ENSO can be examined, as our domain includes a sizable region known to experience the direct effects of both El Niño and the Southern Oscillation or "SO" (see, e.g., Trenberth and Shea 1987). Our analysis thus complements a similar previous analysis of ENSO-related climate variability (Barnett 1991—a complex PCA method was used in the latter case) by focusing on both tropical and extratropical patterns of climatic variability using long data series, albeit omitting some relevant regions from consideration in the process.

The spatiotemporal patterns of the ENSO signals are shown in Fig. 8. The lower- and higher-frequency components (reconstructed with the time-dependent frequency structure indicated by the two dominant bands of Fig. 2a using the procedure described earlier) are both reconstructed for a temperature grid point within the reach of the warm El Niño–cold La Niña tongue and an SLP grid point within the limits of the Indonesian convective region strongly impacted by the Southern Oscillation (Fig. 8a). Both components exhibit highly significant spectral coherence within their respective frequency bands (95%–99% confidence level) with both the SOI and NINO3 indices. These comparisons provide two useful independent, (though neither comprehensive) measures of a relationship with ENSO. For simplicity, we show the spatial evolution for only one (the "low frequency") of the two dominant ENSO-related signals, and for a "composite" cycle obtained as the average pattern of evolution of the signal over the 95-yr period. While certain features differ between the two signal components, the features we focus on below are largely robust between the low- and high-frequency patterns and from cycle to cycle. Low-

frequency and secular changes in the regional influences of ENSO (e.g., Ropelewski and Halpert 1987) may nonetheless represent a real phenomenon and should not be dismissed as stochastic event by event variations, which our methodology largely filters out.

The initial stage shown for both the cold (Fig. 8b) and warm (Fig. 8c) season signal coincide with the peak low phase of the Southern Oscillation (maximum SLP anomaly in the Indonesian convective region, minimum SLP anomaly in the eastern Pacific) in phase with El Niño conditions (maximum positive SST anomalies along the eastern tropical and subtropical Pacific coast). Consistent with other studies (e.g., Horel and Wallace 1981) the low phase of the Southern Oscillation is observed to accompany notable cold-season circulation anomalies over the North Pacific and North America. The cold-season pattern (Fig. 8b) over North America during this positive ENSO phase—for example, roughly the first two stages shown—most closely resembles the Tropical–Northern Hemisphere (TNH) pattern that recent studies have shown to be a characteristic cold-season extratropical teleconnection of ENSO (Livezey and Mo 1987), with patterns resembling the NAO (e.g., Rogers 1984) and Western Pacific Oscillation (WPO) somewhat evident. There is a predominant tendency for hemisphere-wide warmth at this stage, although cooling is found in certain areas where cold advection is suggested or, in the case of Greenland, cooling under a cold-season high-pressure region is suggestive of enhanced radiational cooling. As the cycle progresses, by the third stage shown (half-way between low–high SO and El Niño–La Nina conditions), the TNH pattern over North America has broken down (although a considerable low pressure anomaly remains over the North Pacific) and temperature anomalies are generally weak. The cycle subsequently progresses to the reverse of the initial phase, associated with high SO, La Niña, a reverse TNH pattern, and predominant coolness over the hemisphere.

The SST anomaly patterns are consistent between, and quite persistent through the warm season (Fig. 8c, also see Fig. 8a), but tropical and extratropical circulation anomalies (including the east–west SLP gradients in the tropical Pacific) are considerably weaker, though roughly consistent in phase. Accordingly, land surface temperatures are lower amplitude

---

FIG. 8. Spatial and temporal pattern of ENSO signal. (a) Time reconstruction for (i) low-frequency component, reference SLP grid point in the tropical western Pacific, (ii) low-frequency component, reference temperature grid point in the eastern tropical Pacific, (iii) high-frequency component, same SLP grid point, (iv) high-frequency, same temperature grid point, (v) sum of interdecadal and both ENSO components, SLP grid point, (vi) sum of interdecadal and both components + secular warming signal, temperature grid point. (b) Composite cold-season spatial pattern of low-frequency ENSO signal spanning one half of the average ~5.4-yr cycle length. The initial snapshot corresponds to peak (El Niño–low SO) ENSO conditions, while the final snapshot corresponds to the opposite (La Nina–high phase of SO) conditions that obtain one-half cycle (i.e., ~2.7 years) later. (c) Composite warm-season spatial pattern of low-frequency ENSO signal.
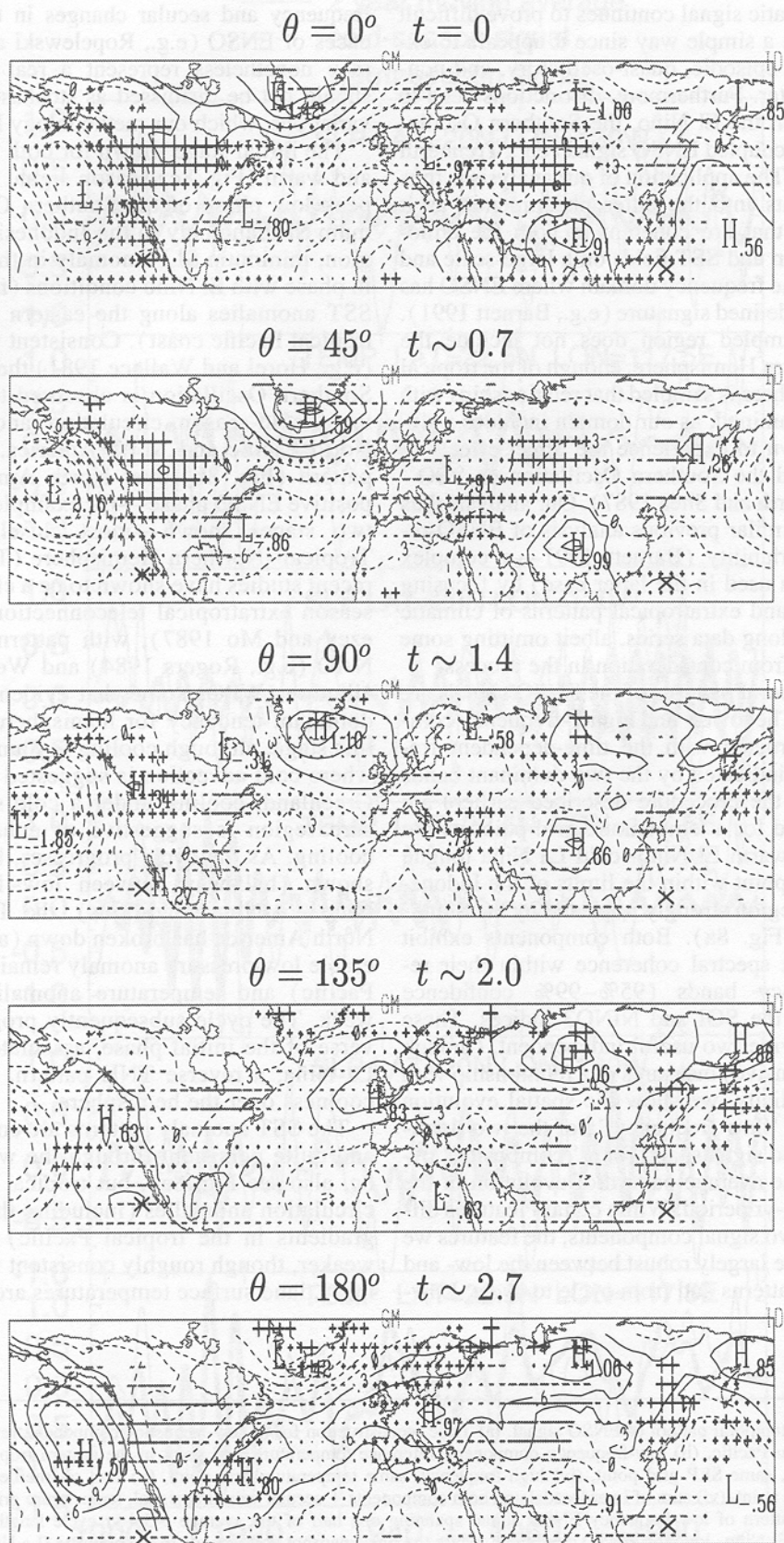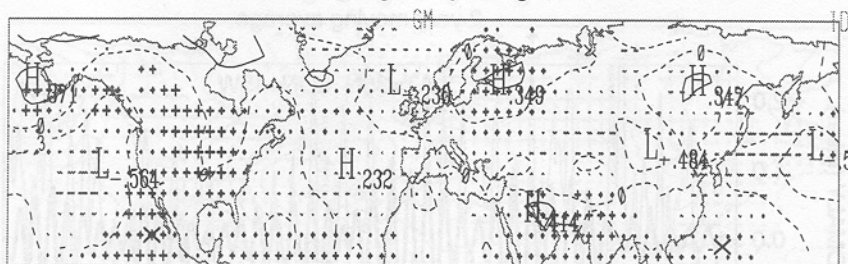
$\theta = 0^o$　　$t = 0$

$\theta = 45^o$　　$t \sim 0.7$
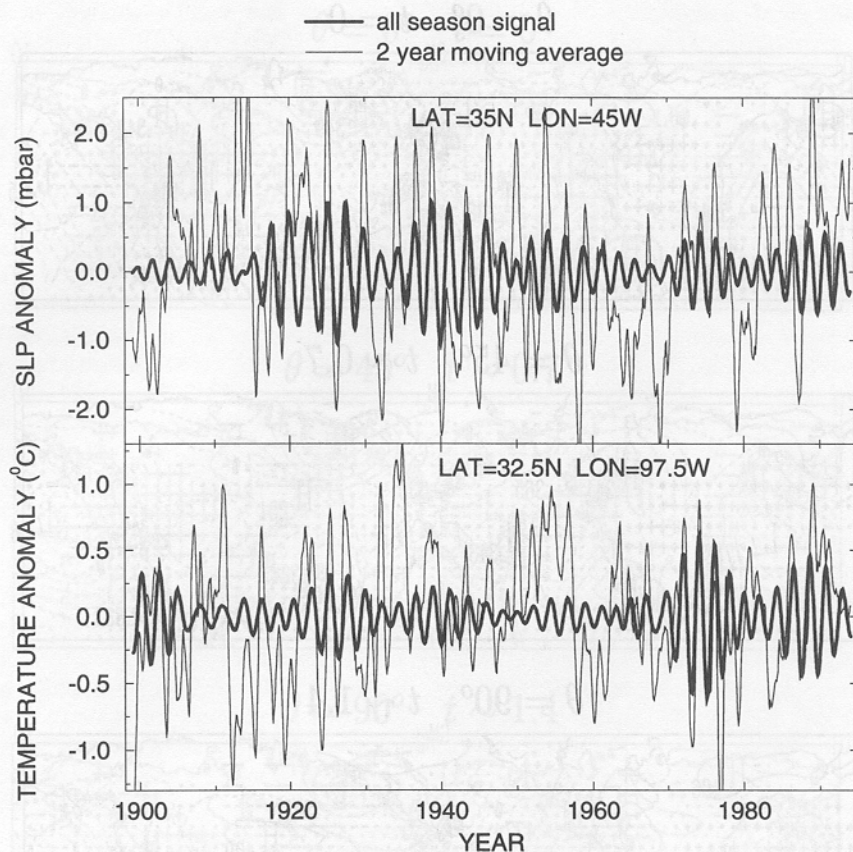

$\theta = 90^o$　　$t \sim 1.4$

$\theta = 135^o$　　$t \sim 2.0$

$\theta = 180^o$　　$t \sim 2.7$

FIG. 8. (*Continued*)

$$\theta = 0^o \quad t = 0$$

$$\theta = 45^o \quad t \sim 0.7$$

$$\theta = 90^o \quad t \sim 1.4$$

$$\theta = 135^o \quad t \sim 2.0$$

$$\theta = 180^o \quad t \sim 2.7$$

FIG. 8. (*Continued*)

FIG. 9. Spatial and temporal pattern of QBO signal. (a) Time reconstruction for all months for (i) reference SLP grid point in central subtropical North Atlantic and (ii) reference temperature grid point in western Soviet Union. (b) Composite cold-season spatial pattern, spanning one-half of the average ~2.2-yr cycle length. The initial snapshot corresponds to the peak positive NAO pattern over the North Atlantic.

and in places of opposite sign (e.g., central Asia) where circulation anomalies and associated surface temperature patterns differ considerably between seasons. The seasonal persistence of the signal thus appears to arise largely from the seasonal robustness of tropical SST anomalies during the evolution of the signal, with circulation anomalies more seasonally variable.

Consistent with the notion of nonstationarity in the patterns of ENSO, we note that the relative signature of El Niño versus SO characteristics is somewhat variable over time for the higher-frequency ENSO component, as evident in the high amplitude early temperature fluctuations in the tropical eastern Pacific contrasting with relatively high-amplitude SLP fluctuations in the western tropical Pacific late in the record (Fig. 8a). Nonetheless, the consistent phase relationship (roughly zero lag) between these SLP and temperature variations indicates a consistent "ENSO" signal. Studies of long-term proxy data suggest considerable nonstationarity in the characteristics of ENSO over several centuries (Cole et al.

1993; Linsley et al. 1994; Dunbar et al. 1994; Bradley et al. 1994).

f. Quasi-biennial mode

Organized quasi-biennial (~2.2-yr period) variability has been observed in North Atlantic winds and sea surface temperature (Deser and Blackmon 1993), north–south variations in United States temperature (Dettinger et al. 1995), Northern Hemisphere SLP (Trenberth and Shin 1984), and globally distributed surface temperature anomalies (MP94). In the latter study, the associated pattern appeared to suggest a strong NAO component that is consistent with the observations of Trenberth and Shin (1984). The joint-mode analysis confirms the association of large-scale quasibiennial variability exhibiting a distinct NAO pattern and indicates hemisphere-wide teleconnections. The pattern of temperature variability is similar to that of MP94, while the associated pattern of SLP variability shows characteristics in common with the observations of Trenberth and Shin (1984). The time-do-
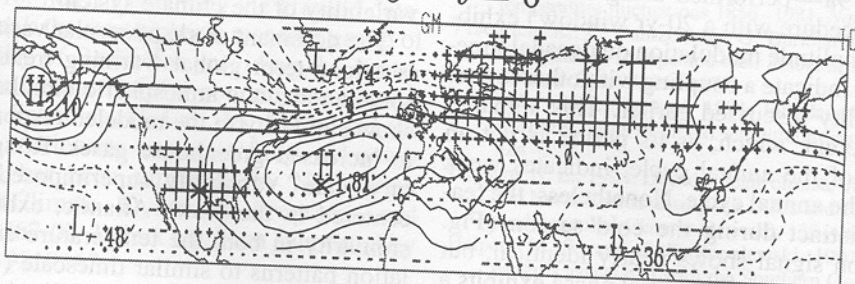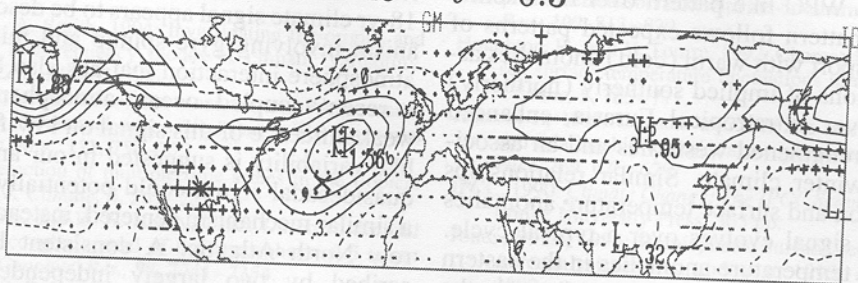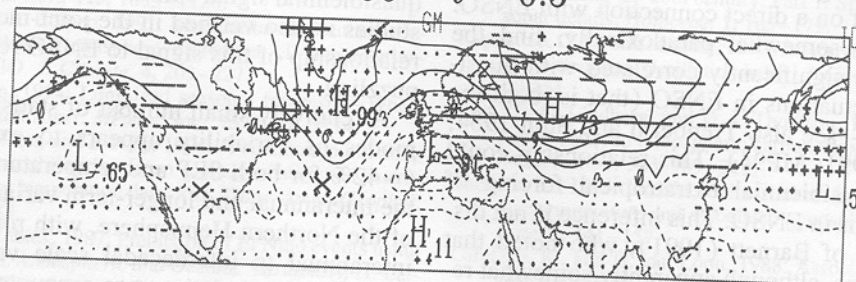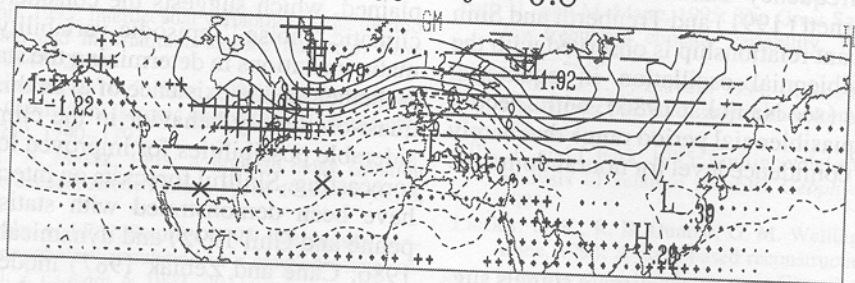
θ = 0°　t = 0

θ = 45°　t ~ 0.3

θ = 90°　t ~ 0.5

θ = 135°　t ~ 0.8

θ = 180°　t ~ 1.1
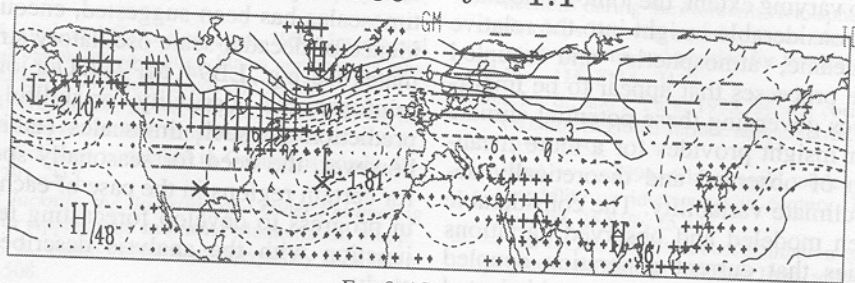
FIG. 9. (Continued)

main signal (Fig. 9a—performed using the evolutive reconstruction procedure with a 20-yr window) exhibits considerable amplitude modulation on decadal timescales, which may indicate a coupling with other lower-frequency variability discussed earlier. This signal is highly phase-coherent, which, as its period is not an integral multiple of the annual cycle, indicates weak phase-locking to the annual cycle. Nonetheless, the features are most distinct during the cold season (Fig. 9b—the all-season signal shows nearly identical, but lower-amplitude, features). The initial phase exhibits a high-amplitude positive NAO pattern over the Atlantic, and a "lopsided" WPO-like pattern over the Pacific. The temperature pattern follows expected patterns of sensible heat transport with warm (cold) anomalies associated with regions of implied southerly (northerly) advection and, over extratropical Eurasia, enhanced warmth due to strengthened westerlies and an associated moderated winter climate. Similar relationships between circulation and surface temperature anomalies are found as the signal evolves over a typical cycle. The lack of large temperature anomalies in the eastern Pacific or any sizeable east–west SLP gradients in the tropical Pacific during the evolution of the signal would seem to cast doubt on a direct connection with ENSO. However, we *do*, somewhat paradoxically, find the QBO signal to be significantly correlated with quasibiennial band fluctuations in ENSO (that is, both the SOI and NINO3—see also Trenberth and Shin 1984; Barnston et al. 1991; MP94). This relationship could thus reflect a quasibiennial extratropical forcing of weaker fluctuations in ENSO. This inference is not dissimilar from that of Barnett (1991), who noted that QB-band variations, although apparently somewhat related to ENSO, had a far weaker loading in the tropical Pacific than low-frequency band ENSO variability. Consistent with Barnett (1991) and Trenberth and Shin (1984), no significant relationship is observed with the stratospheric quasibiennial oscillation in equatorial stratospheric winds (see Naujokat 1986), with spectral coherences in the quasibiennial period range that barely breach the median confidence level for nonrandomness.

5. Discussion

While each of the low-frequency climate signals suggested in our analysis has been observed and studied in previous work to varying extent, the joint-mode analysis does provide considerable insight into the relative importance of oceanic, atmospheric, and coupled ocean–atmosphere processes that appear to be important in the dynamics governing these potential climate signals. This latter insight provides for a more meaningful comparison of observed and theoretically described modes of climate variability. The considerable agreement between modeled and observed variations furthermore implies that current generation coupled ocean–atmosphere models may be sophisticated

enough to capture much of the observed low-frequency variability of the climate system.

The dominant mode of secular variation in our study is a long-term global warming trend associated with some anomalous atmospheric circulation patterns that show similarity to the modeled response of the climate to increased greenhouse gases. Roughly 75-yr "century-scale" variability, superimposed on this trend and centered in the North Atlantic, exhibits considerable similarity in both the temperature and inferred circulation patterns to similar timescale (40–60-yr period) oscillations attributed to variability in the thermohaline circulation in a recent simulation. An interdecadal 16–18-yr climate signal appears to be described by a mechanism involving gyre spinup and midlatitude ocean–atmosphere interaction that has also been predicted in a recent coupled ocean–atmosphere simulation. A weak influence of this signal on low-frequency ENSO-like variability is suggested in our analysis. A weaker quasidecadal signal could potentially be described by a similar mechanism centered, instead, in the more narrow North Atlantic. A consistent ENSO signal described by two largely independent time-evolving bands of interannual variance is also established. A quasibiennial signal similar to that found in other recent studies is also verified in the joint-mode analysis. The relationship of this signal to ENSO remains somewhat puzzling.

A relatively small number of statistically significant modes of variability appears to explain a sizeable (~42% for both SLP and temperature fields) share of the interannual and longer-term variance in the climate of the Northern Hemisphere, with roughly 22% of the interannual to interdecadal scale variance explained when secular variations are accounted for. This nonetheless leaves a relatively large share of variance unexplained, which suggests the considerable influence of climatic "noise," episodic variability, and abrupt climatic transitions in determining the state of the climate. Nonetheless, the existence of even this modest share of quasi-oscillatory behavior in the climate implies considerable possibilities for improved long-range climate forecasting. Skillful forecasts on interannual timescales have been demonstrated with statistical (e.g., Keppenne and Ghil 1992) and dynamical (e.g., Cane et al. 1986; Cane and Zebiak 1987) models of ENSO (see also the review by Barnston et al. 1994). More recently, the possibility of climatic prediction on decadal timescales has been suggested, encouraged by the evidence of decadal-scale oscillatory structure in the climate (see, e.g., LB94; MP94). Our joint-mode analysis reinforces the possibility for skillful regional climate prediction on such timescales (taking into account, however, the need for seasonally specific forecasting for certain regions in the case of each signal). Work is in progress to develop forecasting techniques in conjunction with the analysis described in the present study.

REFERENCES

Allen, M. R., and L. A. Smith, 1994: Investigating the origins and significance of low-frequency modes of climatic variability. *Geophys. Res. Lett.,* **21,** 883–886.

Barnett, T. P., 1983: Interaction of the monsoon and Pacific trade-wind systems at interannual time scales. Part I: The equatorial zone. *Mon. Wea. Rev.,* **111,** 756–773.

——, 1991: The interaction of multiple time scales in the tropical climate system. *J. Climate,* **4,** 269–281.

——, A. D. Del Genio, and R. A. Ruedy, 1992: Unforced decadal oscillations in a coupled model of the atmospheric and ocean mixed layer. *J. Geophys. Res.,* **97,** 7341–7354.

Barnston, A. G., and R. E. Livezey, 1987: Classification, seasonality and persistence of low-frequency atmospheric circulation patterns. *Mon. Wea. Rev.,* **115,** 1083–1126.

——, ——, and M. S. Halpert, 1991: Modulation of Southern Oscillation—Northern Hemisphere midwinter climate relationships by the QBO. *J. Climate,* **4,** 203–227.

——, and Coauthors, 1994: Long-lead seasonal forecasts—Where do we stand? *Bull. Amer. Meteor. Soc.,* **75,** 2097–2114.

Bradley, R., M. E. Mann, and J. Park, 1994: A spatiotemporal analysis of ENSO variability based on globally distributed instrumental and proxy temperature data. *Eos, Trans. Amer. Geophys. Union,* **75,** p. 383.

Cane, M., and S. E. Zebiak, 1987: Prediction of El Nino events using a physical model. *Atmospheric and Oceanic Variability,* H. Cattle, Ed., Royal Meteorological Society Press, 153–182.

——, and S. C. Dolan, 1986: Experimental forecasts of El Niño. *Nature,* **321,** 827–832.

Chen, F., and M. Ghil, 1995: Interdecadal variability of the thermohaline circulation and high-latitude surface fluxes. *J. Phys. Oceanogr.,* **25,** 2547–2568.

Cole, J. E., R. G. Fairbanks, and G. T. Shen, 1993: Recent variability in the Southern Oscillation: Isotopic results from a Tarawa atoll coral. *Science,* **260,** 1790–1793.

Darby, M. S., and L. A. Mysak, 1993: A boolean delay equation model of an interdecadal Arctic climate cycle. *Climate Dyn.,* **8,** 241–246.

Delworth, T., S. Manabe, and R. J. Stouffer, 1993: Interdecadal variations of the thermohaline circulation in a coupled ocean–atmosphere model. *J. Climate,* **6,** 1993–2011.

Deser, C., and M. Blackmon, 1993: Surface climate variations over the North Atlantic Ocean during winter: 1900–1989. *J. Climate,* **6,** 1743–1753.

Dettinger, M. D., M. Ghil, and C. L. Keppenne, 1995: Interannual and interdecadal variability in United States surface–air temperatures, 1910–1987. *Climate Change,* **31,** 36–66.

Dunbar, R. B., G. M. Wellington, M. W. Colgan, and P. W. Glynn, 1994: Eastern Pacific sea surface temperature since 1600 A.D.: The δ^{18} record of climate variability in Galapagos corals. *Paleoceanogr.,* **9,** 291–315.

Efron, B., 1990: *The Jacknife, the Bootstrap and Other Resampling Plans.* Society for Applied and Industrial Mathematics, 92 pp.

Elsner, J. B., and A. A. Tsonis, 1994: Low frequency oscillation. *Nature,* **8,** 507–508.

Folland, C. K., D. E. Parker, and F. E. Kates, 1984: Worldwide marine temperature fluctuations 1856–1981. *Nature,* **310,** 670–673.

Fraedrich, K., C. Bantzer, and U. Burkhardt, 1993: Winter climate anomalies in Europe and their associated circulation at 500 hPa. *Climate Dyn.,* **8,** 161–175.

Ghil, M., and R. Vautard, 1991: Interdecadal oscillations and the warming trend in global temperature time series. *Nature,* **350,** 324–327.

Graham, N. E., 1994: Decadal-scale climate variability in the tropical and North Pacific during the 1970s and 1980s: Observations and model results. *Climate Dyn.,* **10,** 135–162.

Halpert, M. S., and C. F. Ropelewski, 1992: Surface temperature patterns associated with the Southern Oscillation. *J. Climate,* **5,** 577–593.

Horel, J. D., and J. M. Wallace, 1981: Planetary-scale atmospheric phenomena associated with the Southern Oscillation. *Mon. Wea. Rev.,* **109,** 813–829.

Houghton, R., and Y. Tourre, 1992: Characteristics of low-frequency sea surface temperature fluctuations in the tropical Atlantic. *J. Climate,* **5,** 765–771.

Hurrell, J., 1995: Decadal trends in the North Atlantic Oscillation and relationship to regional temperature and precipitation. *Science,* **269,** 676–679.

IPCC, 1990: *Climate Change: The IPCC Scientific Assessment.* Cambridge University Press, 365 pp.

Jones, P. D., 1994: Hemispheric surface temperature variations: A reanalysis and an update to 1993. *J. Climate,* **7,** 1794–1802.

——, and K. R. Briffa, 1992: Global surface air temperature variations during the 20th century. Part 1: Spatial, temporal and seasonal details. *Holocene,* **1,** 165–179.

Keppenne, C. L., and M. Ghil, 1992: Adaptive filtering and prediction of the Southern Oscillation index. *J. Geophys. Res.,* **97,** 20 449–20 454.

Kuo, C., C. Lindberg, and D. J. Thomson, 1990: Coherence established between atmospheric carbon dioxide and global temperature. *Nature,* **343,** 709–713.

Kushnir, Y., 1994: Interdecadal variations in North Atlantic sea surface temperature and associated atmospheric conditions. *J. Climate,* **7,** 141–157.

Labitzke, K., and H. van Loon, 1988: Associations between the 11-year solar cycle, the QBO, and the atmosphere. Part I: The troposphere and stratosphere in the Northern Hemisphere in winter. *J. Atmos. Terr. Phys.,* **50,** 197–206.

Lall, U., and M. Mann, 1995: The Great Salt Lake: A barometer of low-frequency climatic variability. *Water Resour. Res.,* **31,** 2503–2515.

Latif, M., and T. P. Barnett, 1994: Causes of decadal climate variability over the North Pacific and North America. *Science,* **266,** 634–637.

Lilly, J., and J. Park, 1995: Multiwavelet spectral and polarization analysis of seismic records. *Geophys. J. Int.,* **122,** 1001–1021.

Linsley, B. K., R. B. Dunbar, G. M. Wellington, and D. A. Mucciarone, 1994: A coral-based reconstruction of intertropical convergence zone variability over Central America since 1707. *J. Geophys. Res.,* **99,** 9977–9994.

Livezey, R. E., and K. C. Mo, 1987: Tropical–extratropical teleconnections during the Northern Hemisphere winter. Part II: Relationships between monthly mean Northern Hemisphere circulation patterns and proxies for tropical convection. *Mon. Wea. Rev.,* **115,** 3115–3132.

Mann, M. E., and J. Park, 1993: Spatial correlations of interdecadal variation in global surface temperatures. *Geophys. Res. Lett.,* **20,** 1055–1058.

——, and ——, 1994: Global-scale modes of surface temperature variability on interannual to century timescales. *J. Geophys. Res.,* **99,** 25 819–25 833.

——, and J. Lees, 1996: Robust estimation of background noise and signal detection in climatic time series. *Climate Change,* in press.

——, U. Lall, and B. Saltzman, 1995a: Decadal-to-centennial-scale climate variability: Insights into the rise and fall of the Great Salt Lake. *Geophys. Res. Lett.*, **22**, 937–940.

——, J. Park, and R. Bradley, 1995b: Global interdecadal- and century-scale oscillations during the past five centuries. *Nature*, **378**, 266–270.

Marshall, S., M. E. Mann, R. J. Oglesby, and B. Saltzman, 1995: A comparison of the CCM1-simulated climates for pre-industrial and present-day CO$_2$ levels. *Glob. Planet. Change*, **10**, 163–180.

Mehta, V. M., and T. Delworth, 1995: Decadal variability of the tropical Atlantic ocean surface temperature in shipboard measurements and in a global ocean–atmosphere model. *J. Climate*, **8**, 172–190.

Miller, A. J., D. R. Cayan, T. P. Barnett, N. E. Graham, and J. M. Oberhuber, 1994: Interdecadal variability of the Pacific Ocean: Model response to observed heat flux and wind stress anomalies. *Climate Dyn.*, **9**, 287–302.

Mysak, L. A., and S. B. Power, 1992: Sea-ice anomalies in the western Arctic and Greenland–Iceland Sea and their relation to an interdecadal climate cycle. *Climatol. Bull.*, **26**, 147–176.

Naujokat, B., 1986: An update of the observed quasibiennial oscillation of the stratospheric winds over the Tropics. *J. Atmos. Sci.*, **43**, 1873–1877.

Oglesby, R. J., and B. Saltzman, 1992: Equilibrium climate statistics of a general circulation model as a function of atmospheric carbon dioxide. Part I: Geographic distributions of primary variables. *J. Climate*, **5**, 66–92.

Park, J., and K. A. Maasch, 1993: Plio-Pleistocene time evolution of the 100-kyr cycle in marine paleoclimate records. *J. Geophys. Res.*, **98**, 447–461.

——, C. R. Lindberg, and F. L. Vernon III, 1987: Multitaper spectral analysis of high-frequency seismograms. *J. Geophys. Res.*, **92**, 12 675–12 684.

Preisendorfer, R. W., 1988: Principal component analysis in meteorology and oceanography. *Developments, in Atmospheric Science*, Elsevier, 425 pp.

Rogers, J. C., 1984: The association between the North Atlantic Oscillation and the Southern Oscillation in the Northern Hemisphere. *Mon. Wea. Rev.*, **112**, 1999–2015.

Ropelewski, C. F., and M. S. Halpert, 1987: Global and regional scale precipitation patterns associated with the El Niño–Southern Oscillation. *Mon. Wea. Rev.*, **115**, 1606–1626.

——, ——, and X. Wang, 1992: Observed tropospheric biennial variability and its relationship to the Southern Oscillation. *J. Climate*, **5**, 594–614.

Royer, T. C., 1993: High-latitude oceanic variability associated with the 18.6 year nodal tide. *J. Geophys. Res.*, **98**, 4639–4644.

Schlesinger, M. E., and N. Ramankutty, 1994: An oscillation in the global climate system of period 65–70 years. *Nature*, **367**, 723–726.

Tanimoto, Y., N. Iwasaka, K. Hanawa, and Y. Toba, 1993: Characteristic variations of sea surface temperature with multiple time scales in the North Pacific. *J. Climate*, **6**, 1153–1160.

Thomson, D. J., 1982: Spectrum estimation and harmonic analysis. *Proc. IEEE*, **70**, 1055–1096.

Tinsley, B. A., 1988: The solar cycle and QBO influence on the latitude of storm tracks in the North Atlantic. *Geophys. Res. Lett.*, **15**, 409–412.

Trenberth, K. E., 1990: Recent observed interdecadal climate changes in the Northern Hemisphere. *Bull. Amer. Meteor. Soc.*, **71**, 988–993.

——, and D. A. Paolino, 1980: The Northern Hemisphere sea-level pressure data set: Trends, errors and discontinuities. *Mon. Wea. Rev.*, **108**, 855–872.

——, and W.-T. K. Shin, 1984: Quasibiennial fluctuations in sea level pressures over the Northern Hemisphere. *Mon. Wea. Rev.*, **112**, 761–777.

——, and D. J. Shea, 1987: On the evolution of the Southern Oscillation. *Mon. Wea. Rev.*, **115**, 3078–3096.

——, and J. W. Hurrell, 1994: Decadal atmosphere–ocean variations in the Pacific. *Climate Dyn.*, **9**, 303–319.

——, and T. J. Hoar, 1995: The 1990–1995 El Nino–Southern Oscillation event: Longest on record. *Geophys. Res. Lett.*, **23**, 57–60.

Unal, Y. S., and M. Ghil, 1995: Interannual and interdecadal oscillation patterns in sea level. *Climate Dyn.*, **11**, 255–279.

von Storch, J. S., 1994: Interdecadal variability in a global coupled model. *Tellus*, **46**, 419–432.

Wallace, J. M., C. Smith, and C. S. Bretherton, 1992: Singular value decomposition of wintertime sea surface temperatures and 500-mb height anomalies. *J. Climate*, **5**, 561–576.

Weaver, A. J., E. S. Sarachik, and J. Marotzke, 1991: Freshwater flux forcing of decadal and interdecadal oceanic variability. *Nature*, **353**, 836–838.

Xu, J. S., 1993: The joint modes of the coupled atmosphere–ocean system observed from 1967–1986. *J. Climate*, **6**, 816–838.

Yang, J., and J. D. Neelin, 1993: Sea–ice interaction with the thermohaline circulation. *Geophys. Res. Lett.*, **20**, 217–220.